1

GROUNDWATER WATER REMEDIATION BY STATIC DIFFUSION USING NANO-ZERO VALENT METALS (Fe^0, Cu^0, Al^0), n-FeH^{n+}, n-$Fe(OH)_X$, n-FeOOH, n-Fe-$[O_XH_Y]^{(n+/-)}$

David D.J. Antia
DCA Consultants Ltd., Scotland, UK

1.1 INTRODUCTION

Zero valent metals (ZVM) and ZVM combinations, including magnetic ZVM [1–4] and reduced ZVM [5–7], are highly efficient water treatment agents [8–12]. They will remove ions, chemicals, compounds, and biota from water. The principal ZVM used in pilot and commercial water treatment are Fe^0 and $Fe^0 + Cu^0$ [13–17]. Prices for ZVM powders are a function of commodity prices, particle size, particle shape (e.g., dendritic, spherical, platy, irregular, etc), manufacturing method, source, and quantity ordered. Current (June 2014) prices (k$ FOB t^{-1}) for powders are (i) 13,000–400,000 nm (Fe = 0.6–1.6; Cu = 1–7; Al = 5–20), (ii) <3,000 to >8,000 nm (Fe = 5–15; Cu = 9–18; Al = 9–850), (iii) 10–1000 nm (Fe = 30–1100; Cu = 9–1000; Al = 9–900). n-ZVM powders are either used to treat water in a reactor [10], or are injected into an aquifer [10, 17], or are placed in a permeable reactive barrier (PRB) within the aquifer [10, 18].

Use of n-ZVM in a fixed (packed) bed reactor (where all the feed water flows through the n-ZVM) is impractical, as n-Fe^0 rapidly corrodes and expands to form hydrated, low-density hydroxides ($Fe(OH)_2$, $Fe(OH)_3$) and peroxides (FeOOH). This results [10] in a decrease in porosity, decrease in permeability, increase in the proportion of dead end pores, and a decrease in pore throat size. Associated gas bubble formation (O_2, H_2 [10]) results in permeability reduction [18, 19] due to gas occlusion switching water flow from viscous flow to Knudsen diffusion [20–22]. The net effect is a major reduction in permeability (and water flow rate) over a short time period (Fig. 1.1a) in the reactor, or aquifer [10]. Fluid flow (Q_f, $m^3\ m^{-2}\ s^{-1}$) = $k_p\ D_f$ [20–22]. A list of abbreviations is provided in Appendix 1.A. The dominant fluid flow mechanism switches over a period of 2–6 weeks from viscous flow to Knudsen diffusion due to the generation and presence of trapped nano/micron-sized gas bubbles [10, 20–22].

Changing the reactor type to a diabatic diffusion reactor (where a body of water overlies a static body of ZVM, and all water enters and leaves the reactor through the water body), mimics the situation that occurs in an aquifer, during remediation, following n-ZVM injection. A policy of groundwater abstraction, treatment, and reinjection allows the remediation to be undertaken in a short time period in a controlled environment without creating long-term damage to the aquifer [10]. In an unconfined, diabatic, diffusion environment (e.g., shallow contaminated aquifer or soil), the principal controls on Eh, pH, EC (electrical conductivity), and remediation are [10]: (i) flowing water space velocity ($SV = Q_{fr}/W_{zvm}$); (ii) the stored water to ZVM ratio, [$SWZ = S_w/W_{zvm}$]; (iii) the water composition; (iv) atmospheric/groundwater temperature fluctuations; (v) atmosphere composition variation (principally humidity); (vi) atmospheric pressure fluctuation; (vii) vertical infiltration recharge (associated with storm events) into the aquifer/soil; (viii) water losses from the aquifer/soil, due to evaporation, leaching, and the interaction of the n-ZVM (and n-ZVM products) with minerals and biota; and (ix) porosity occlusion resulting from the movement of displaced air as the water levels rise and fall (during and following infiltration recharge) [20–23].

Nanomaterials for Environmental Protection, First Edition. Edited by Boris I. Kharisov, Oxana V. Kharissova, and H. V. Rasika Dias.

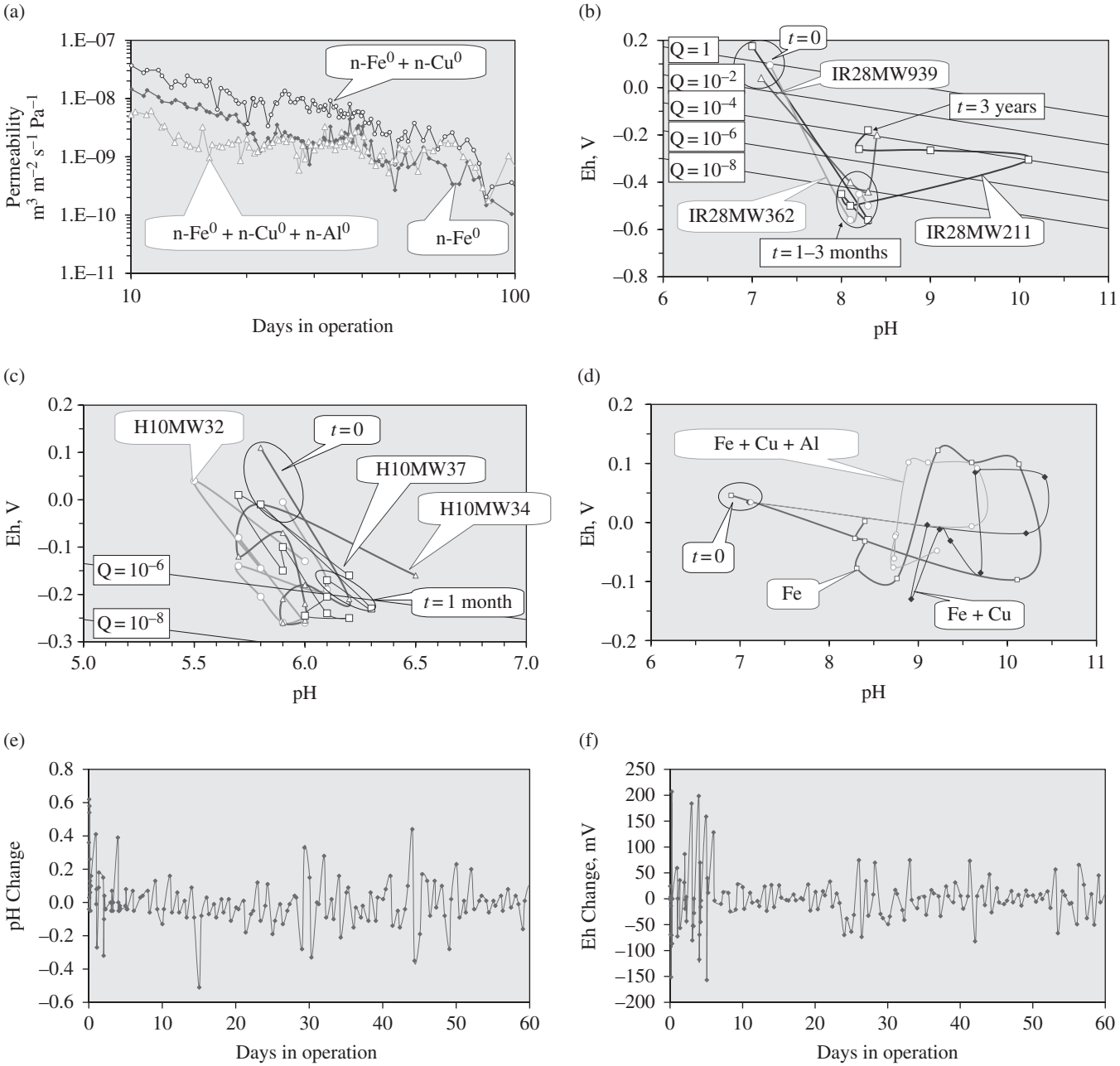

FIGURE 1.1 Nano-Material Behavior During Remediation. (a) n-ZVM permeability decline in a fixed (packed) bed multi-tubular reactor [10]. (b) Impact of 7.2 t, pneumatically injected n-Fe^0 (>1000 nm) into 1839 m^3 soil, on Eh and pH with time. Hunters Point, San Francisco, USA) [17]. Q = equilibrium Mol l^{-1} TCE/DCE; (c) Impact of 7.63 kg infiltrated n-Fe^0 (50–300 nm) (containing 0.15% Pd) into 808 m^3 soil, on Eh and pH with time (12 months): NAS Jacksonville, Florida, USA [17]. (d) n-ZVM: pH vs. Eh over time in a static diffusion reactor showing typical trajectories. Data points taken at 0, 1, 10, 20, 30, 40, 50, 60 day intervals [135]. (e) pH oscillation with time, n-Fe^0[135]. Oscillation value = change in pH from previous measurement. (f) Eh oscillation with time, n-Fe^0: Data: [135]. Oscillation value = change in Eh from previous measurement.

This review considers (i) the contaminants that can be removed by n-Fe^0; (ii) the factors and mechanisms that impact on the remediation rates; (iii) the interaction between n-Fe^0, water, ZVM corrosion/remediation products; and (iv) Eh, pH oscillations, and trajectories and their impact on remediation.

1.2 CONTAMINANTS REMOVED BY n-Fe^0, n-Cu^0, AND n-Al^0

Contaminants removed from water in a diffusion environment at temperatures in the range [<0 to >70°C] by n-Fe^0, n-Cu^0, and n-Al^0, include

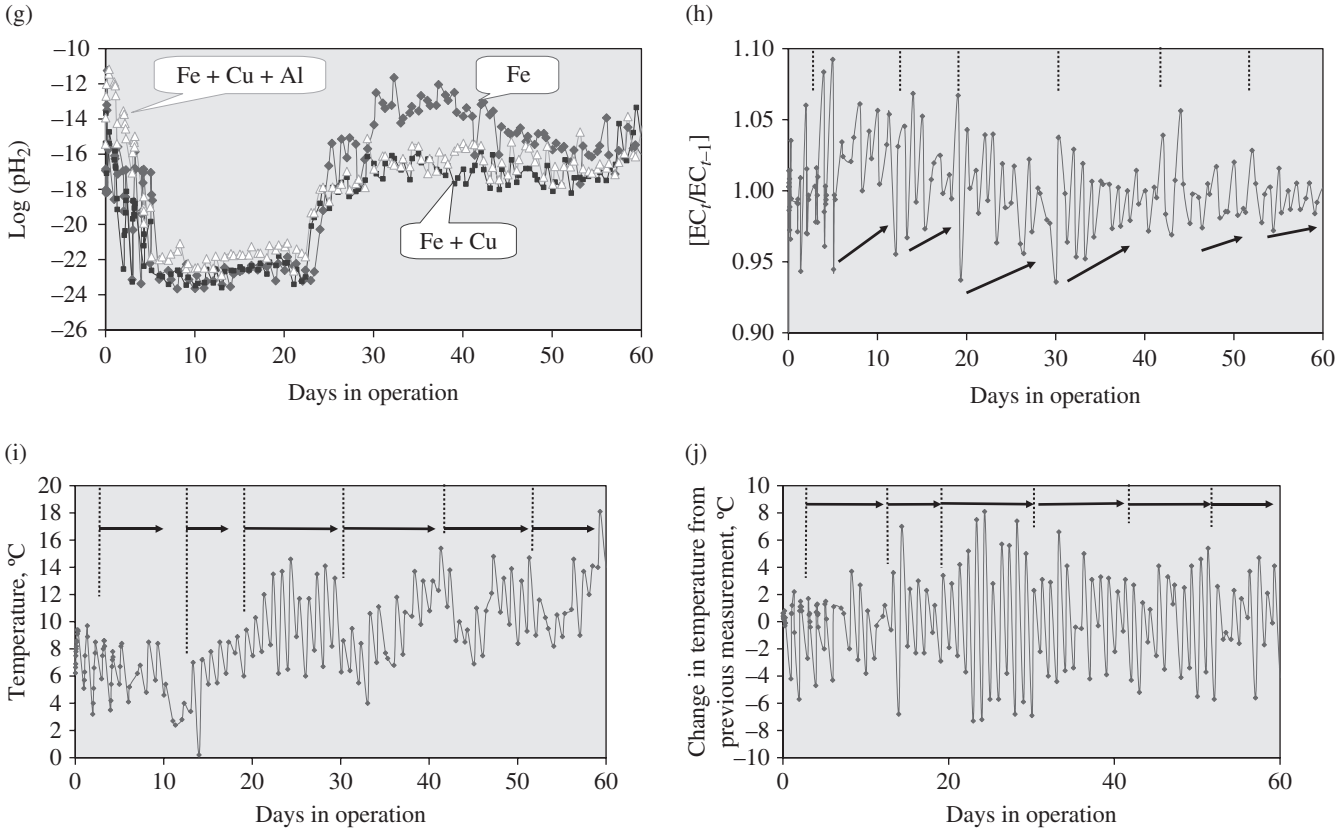

FIGURE 1.1 (*Continued*) (g) pH_2 vs. time in a static diffusion reactor for nano-ZVM (Fig. 1.1e and f). (h) Typical declining EC oscillations with time. n-Fe^0 [135]. (i) Variation in temperature with time (Figs. 1.1e–h) (j) Temperature oscillations with time.

1. Pollutants of the form MO_x, where M = S, N, C, P, Cl (e.g., nitrates [24–30], nitrites [30–33], perchlorates [34–37], carbonic acids [38–45], phosphates [46], sulfates [47–50]). Pollutants are removed within green rust, or ZVM-hydroxide/peroxide structures, or polyoxometallate (POM) structures, by cation/anion substitution, or by layer accretion [38–50]. Green rusts are highly reactive structures comprising [38–50] alternating positively and negatively charged hydroxide/peroxide layers and hydrated anion layers with the general composition $[Cation_a^{I}Cation_c^{II}Cation_b^{III}(OH)_m(OOH)_d]^{x+}[(A_{y/nv}\ yiH_2O]^{x-}$. Cations and anions can be substituted [38–50]. *A* is an anion (e.g., Cl^-, SO_4^{2-}, CO_3^{2-}, Br^-, I^-, NO_3^-, ClO_4^-, SO_3^{2-}, SeO_4^{2-}, PO_4^{2-}, OH^-, OOH^-, O_x^{y-}, etc.); nv = valency; yi = the inter-layer water and is typically between 2 and 4. A typical green rust forms as plates 5–2000 nm in diameter and about 40 nm thick, for example, [50]. Green rusts (ZVM degradation products) are highly efficient anion and cation scavengers and may be as reactive, or more reactive, than Fe^0 [9, 49]. During scavenging operations, the "green rusts" can incorporate cation layers of the form $[Cation_e^{I}(OH)_m(OOH)_d]^{x+}$ and $[Cation_f^{IV}(OH)_m(OOH)_d]^{x+}$ and higher valent cation hydroxides/peroxides.
2. Gases, including H_2S [51], O_2 [52], CO_2 [53], CO [53], H_2 [53].
3. Halogenated ions of the form $[halogen]_xO_y$ (e.g., chlorates, bromates, perchlorates, etc.), and $C_x[Halogen]_yO_z$ [34–37] and halogenated organic compounds of the general form $C_xH_y[Halogen]_z$, where *y* can be 0. The halogen is one or more of Cl, Br, I, F. [54–57], for example, chloromethane (CM), trichloromethane (TCM), dichloromethane (DCM), tetrachloromethane; perchloroethylene (PCE), trichloroethylene (TCE), dichloroethylene (DCE); vinyl chloride (VC); hexachloroethane, tetrachloroethane, trichloroethane, dichloroethane, chloropropane (etc.), chlorobutane (etc.), chlorobenzene, (etc.), ethylene dibromide (EDB), perchlorate, polychlorinated biphenyls (PCB's). The end degradation products take the generic form C_xH_y (e.g., methane, ethyne, ethene, ethane, propane, butane, pentane, hexane, heptane, octane). These may be further altered to form products of the form: $H_xC_yO_z$ or ring structures.
4. Organic peroxides (e.g., triacetone triperoxide (TATP))[58].
5. Organic nitrogenous compounds, including azo dyes [59–61], atrazine [62, 63], cyclonite/hexogen (RDX) [14, 64], dinitrotoluene (DNT) [65, 66], nitrosodimethylamine (NDMA) [67, 68], nitrocellulose [69], tetramethylenetetranitramine (HMX) [70–72], trinitrotoluene (TNT) [73–75], disinfection by-products (DBPs) [76, 77], fertilizers [78, 79], pesticides [80–83], herbicides [84, 85], fungicides [86].

6. Organic compounds including Methyl *tert*-butyl Ether (MTBE) [87], aromatics (e.g., BTEX) [88–91]), hydrocarbons [21, 92–98], hormonal pollutants [99]. Metal carbonyl pollutants (e.g., $Fe(CO)_5$, $Fe(CO)_4$) can be reduced to n-Fe^0 (5–15 nm) by thermolysis in the presence of functional polymers [100].
7. Most metals, metalloids, and nonmetals, including their oxides, hydrides, hydroxides, peroxides, nitrates, nitrites, sulfides, sulfates, halides, carbonates, bicarbonates, and phosphates. ZVM is used to adjust the Eh and pH. This shifts the water redox environment into a redox environment, which will allow either direct precipitation, or precipitation by substitution of Fe in a precipitated Fe corrosion product [10, 101–113]. Examples of contaminant ions and the associated precipitated products, which can be formed by the presence of ZVM, are summarized in Appendix 1.B.
8. Microbiota [10, 114–128] including *Escherichia coli* [115–118, 123, 124, 128], colliforms (e.g., *Enterococcus faecium*, *Enterococcus faecilis*) [128], *Klebsiella pneumoniae* [125], *Salmonella typhimurium* [10], *Salmonella enterica* [124], *Salmonella paratyphi* [125], *Shigella* spp. [125], *Salmonella* spp.[124], *Staphylococcus aureus* [117, 118], *Streptococci* spp. [126], *Bacillus cereuis* [118], *Bacillus subtilis var. niger* [116, 119, 123], *Dehalococcoides* spp. [123], *Pseudomonas spp.* [118], *Pseudomonas fluorescens* [116, 118, 123], *Pseudomonas aeruginosa* [125], *Vibrio parahaemolyticus* [118], *Vibrio cholerae* [126], phiX174/FX174 [120, 128], T1 [121], Aichi virus [120], adenovirus 41 [120], MS-2 [116, 120, 128], Hepatitis A [122], norovirus [122], rotavirus [122], f2 virus [128], *Alcaligenes eutrophus* [123], *Aspergillus versicolor* [116, 119, 122], *Cryptosporidium* spp. [126], *Naeglaeria* spp. [126], *Naeglaeria fowleri* [128], *Giardia* spp. [126], *Hartmannella veriformis* [128], *Tetrahymena pyriformis* [128], *Daphnia magna* [116], *Pseudokirchneriella subcapitata* [116], *Dunaliella tertiolecta* [116], *Thalassiorsria pseudonana* [116], *Isochrysis galbbana* [116], fungi [127], prions [127], viruses [127], protozoa [127], bacteria [127], algae [127], etc. n-Fe^0 (20–30 nm) rapidly inactivates microorganisms by coating them with Fe(OOH) [119]. Inactivation is by one or more of Eh:pH changes and the interaction of Fe corrosion products (oxides, hydroxides, and peroxides), for example, [114, 119].
9. Macrobiota. n-Fe^0 in soil (0.1 to >1 g n-Fe^0 kg^{-1} soil) adversely affect worms (e.g., *Eisenia fetida* and *Lumbricus rubellus*) and springtails (e.g., *Folsomnia candida*) [123].
10. Plants. Concentrations of n-Fe^0 in excess of 250 mg kg^{-1} soil have been found to stunt the growth of rye grass and clover [123].

1.3 REMEDIATION MECHANISMS

The mechanisms associated with ZVM remediation are the subject of conflicting, overlapping, and competing hypotheses, and more than one mechanism applies in each remediation environment. The principal hypotheses are

1. *Catalyst Model:* ZVM acts as a Langmuir-Hinshelwood catalyst (e.g., [55, 95], that is, adsorption of reactants on ZVM surface and desorption of products [55, 130, 131]), or Eley-Rideal catalyst (e.g., [95, 129], i.e., adsorption of one or more reactants on the ZVM surface with reaction of the adsorbed species with one or more fluid-phase reactants that are not adsorbed on the ZVM surface to produce a product [129–131]), or acid catalyst (Fe-H^{n+}) [10, 21, 96–98].
2. *Redox Model:* ZVM changes the water Eh and pH, thereby forcing remediation by changing both K and ΔG for the remediation reaction [10]. Under this model, n-ZVM reactions are essentially fluid phase electrochemical reactions, or contact surface reactions [10].
3. *Galvanic Model:* ZVM ionization (Appendix 1.B, Appendix 1.C) results in n-ZVM acting as self-charging galvanic cells (Fig. 1.2) that adjust the water pH and Eh. This adjustment forces a change in the cation:anion equilibrium state within the water [10]. The change in equilibrium state forces the reduction/oxidation of specific cations and anions, and a change in the Gibbs Free Energy associated with the remediation reaction [103, 104]. The presence of ZVM (and ZVM-ion adducts) in water creates (in a diabatic environment) a perpetual oscillation between higher and lower Eh and higher and lower pH [10] (Fig. 1.1b–j). This oscillation, which can be interpreted as alternating charging and discharging of the galvanic cells (Fig. 1.2): (i) creates, discharges, and adsorbs H^+ (protons, H_3O^+, $H_5O_2^+$, $H_7O_3^+$, $H_9O_4^+$, FeH^{2+}, FeH_2^+), e^- (H^-, H_2O^-, electrons), O^-, O^{2-}, O_2^-, H_2O_2, OH, OH^-, O_2H, and O_2H^-; (ii) creates a unique (ZVM specific) trajectory of Eh/pH change with both residence time and space velocity [10]. This galvanic discharge–recharge mechanism results in substantial water consumption (>0.18 *t* H_2O t^{-1} n-Fe^0), but drives fluid phase (and ZVM/ion surface) Fenton Reactions, electron shuttle reactions, proton shuttle reactions, and oxide ($H_xO_y^{(c+/-)}$) shuttle reactions within water [10, 96]. These reactions undertake the reduction/oxidation of pollutants,

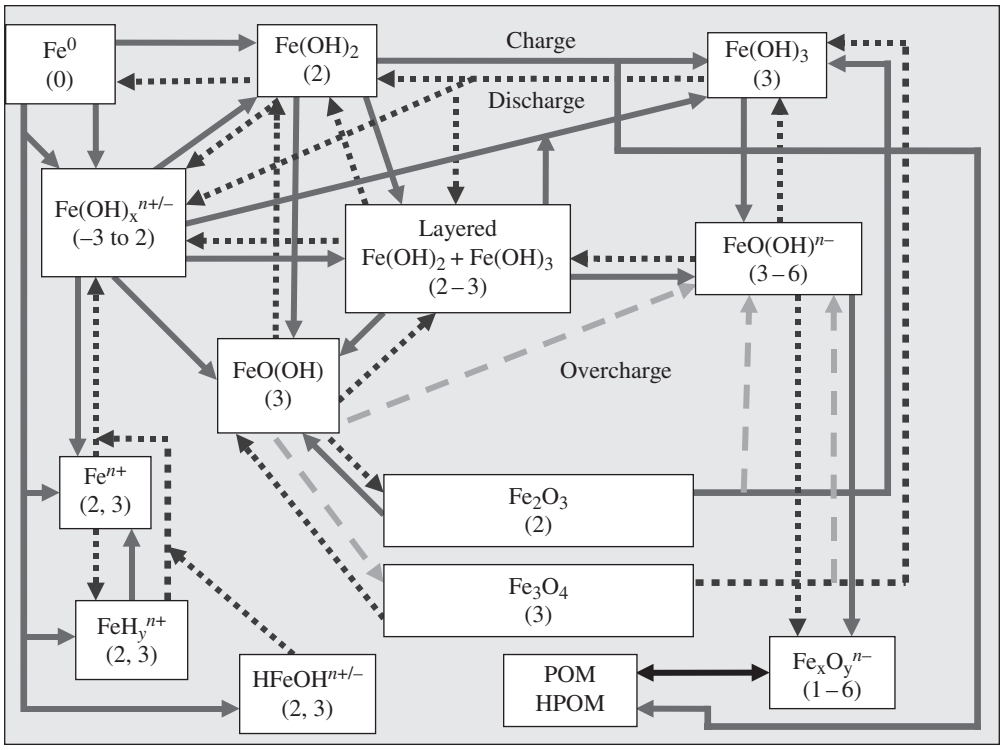

FIGURE 1.2 Fe–Hydrogen Redox Cell: Simplified relationship between n-Fe^0, Fe^0 products, oxidation number (brackets), and stored charge in the various ZVM components.

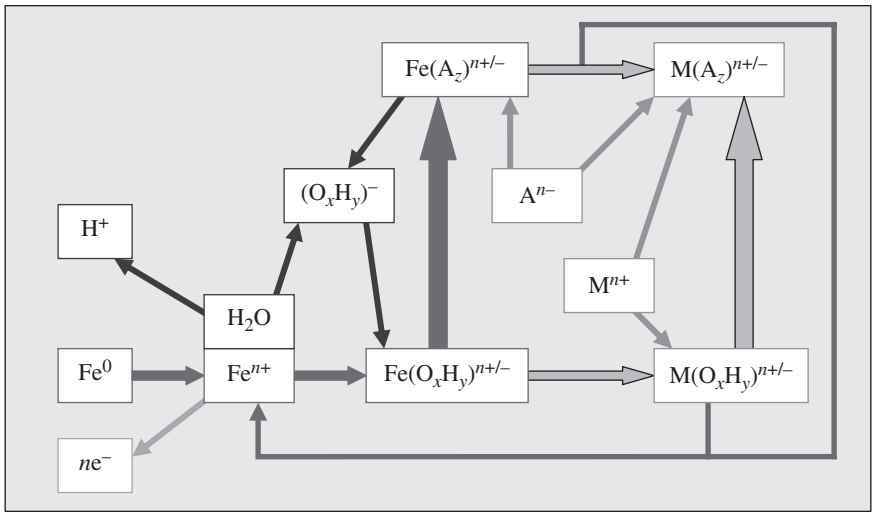

FIGURE 1.3 Fe-water Redox cell, simplified sequence of anion and cation exchange.

removal by incorporation into hydroxide/peroxide precipitates of anions and cations, and the reformulation of organic pollutants into simple alkanes and alkenes [10, 21, 95–98].

4. *Adsorption Model*: ion substitution (Fig. 1.3) of ZVM corrosion products and nano–molecular growth in self-assembly molecules nucleating around ZVM corrosion products results in the removal (by substitution/adsorption) of pollutant ions [38–50, 101, 102]. This model is treated in this study as a subset (Figs. 1.2 and 1.3) of the Galvanic Model.

The generic remediation reaction takes the form $aA+bB=dD+eE$. If $C_{t=0}$ = the contaminant at time, $t=0$, then the observed rate of reaction ($k_{observed}$), between $t=0$, and $t=m$, can be determined [130, 131] as

$$k_{\text{observed}} = \frac{\left(C_{t=m} / C_{t=0}\right)}{(t = m(\text{s}))} \tag{1.1}$$

$$\text{Ln}\left(\frac{C_{t=0}}{C_{t=m}}\right) = \left[k_{\text{observed}}\right]t \tag{1.2}$$

Equations 1.1, 1.2 apply to each remediation model.

1.3.1 Catalyst Model

The hypothesis [48] that ZVM acts as a catalyst will result in decreasing particle size, increasing particle surface area, and/or increasing the quantity of ZVM, automatically increasing the observed rate of reaction ($k_{observed}$) [48, 55, 129–131]:

$$k_{sa} = \frac{k_{\text{observed}}}{a_{s(t=n)}p_m}[\text{Normalised Reaction Rate}] \tag{1.3}$$

$$k_{sa} = A_{sa}\exp\left(\frac{-E_{a(sa)}}{RT}\right) \tag{1.4}$$

$$k_{\text{observed}} = A_{(\text{observed})}\exp\left(\frac{-E_{a(\text{observed})}}{RT}\right) \tag{1.5}$$

$$\text{Reaction rate}, v, \left(\text{mol}\,\text{l}^{-1}\text{s}^{-1}\right) = k\left[\text{A}\right]^m\left[\text{B}\right]^n\left[\text{C}_a\right]^p \tag{1.6}$$

It is commonly assumed that if a plot of $\ln(k_{sa}$ or $k_{observed})$ vs. time and pollutant concentration can be interpreted as a negative, or positive, zero-, first-, second- or third-order reaction [130, 131], then the ZVM must be acting as a catalyst. However, the primary interaction of the ZVM is with water (e.g., n-$Fe^0 + H_2O = HFeOH^{2+} + 2e^-$), and this interaction generates e^- [103] (Appendix 1.C). e^- is a powerful catalyst (used in electron shuttle reactions) [130]. It is therefore possible that much of the catalytic activity attributed to n-Fe^0 (and other ZVM) has been misattributed, and the actual catalytic activity/remediation reactions are undertaken by e^- [10] (as the availability of e^- is directly linked to the corrosion of ZVM (Appendix 1.B, 1.C)).

The catalytic model assumes that the remediation reactions may take the form, A + ZVM = {A[ZVM]} = products, or A + ZVM hydride, oxide, hydroxide, peroxide = {A[ZVM hydride, oxide, hydroxide, peroxide]} = products, The associated reaction rates are [130]: k_d = A + ZVM = {A[ZVM]}; k_{-d} = {A[ZVM]} = A + ZVM; k_r = {A[ZVM]} = products. The overall rate of reaction (v) = k_r[{A[ZVM]}] = $k_d\ k_r$ [A{ZVM}]/($k_{-d}+k_r$) [130] and the overall rate coefficient $k_{\text{observed}} = v/\{\text{A[ZVM]}\} = k_d k_r/(k_{-d}+k_r)$ [130]. The equilibrium constant ($K_{\{\text{A[ZVM]}\}}$) for the encounter pair {A[ZVM]} is k_d/k_{-d} and $k_{\text{observed}} = k_r\ K_{\{\text{A[ZVM]}\}}$[130].

In groundwater, the ZVM diffusion environment results in $k_{\text{observed}}\ (\text{m}^3\ \text{s}^{-1}) = 4\pi r_{\{\text{A[ZVM]}\}} D_{\{\text{A[ZVM]}\}}$[130]. Transition state theory (absolute rate theory) [130] defines: $k_{\text{observed}} = k_B T/h\ \exp(-\Delta G^{\ddagger}/RT)$. The concentration of dissolved ions in the water impacts directly on the reaction rate (k), that is, $k_{\text{observed}} = (k_B T/h)\ K^{\ddagger}\ (\gamma_A\ \gamma_{ZVM}/\gamma_{\{\text{A[ZVM]}\}})$ [130]. These interactions are rarely accounted for in studies that suggest that ZVM acts as a remediation catalyst.

1.3.2 Redox Model

In groundwater [103, 104, 131]:

$$\Delta E\left(\text{Eh}\right) = \Delta E^{\circ} - \frac{RT}{nF}\ln\left[\text{Q}\right] = \frac{\Delta G}{\left(nF\right)} = -\Delta E^{\circ} - \frac{RT}{nF}\ln\left[\text{K}\right] \tag{1.7}$$

$$\Delta E^{\circ} = \frac{RT}{nF}\ln\left[\text{K}\right] = \frac{\Delta G^{\circ}}{\left(nF\right)} \tag{1.8}$$

A non-catalytic redox remediation reaction can be expressed as $a[A]+mH^{+}+ne^{-}=b[B]+c[H_2O]$. This generic equation allows the relationship between Eh, pH, E, ΔG°, and $([B]^{b}/[A]^{a})$ associated with each remediation reaction to be summarized [103, 131] as

1. when A is an aqueous ion (oxide, hydroxide, peroxide) and B is a precipitate as $Eh=\Delta G^{\circ}/(nF)+(0.0591/n)\log([B]^{b}/[A]^{a})+([-0.0591m/n\ [pH]])$; where $\Delta G^{\circ}/(nF)=\Delta E^{\circ}=-RT\ln[K]$: $pH=-\log H^{+}$; $(H_2O)^{c}=1$
2. when [A] and [B] are dissolved substances (M L^{-1}), and $m>0$ and $n=0$, then, $\log([B]^{b}/[A]^{a})=\Delta E^{\circ}+m[pH]$
3. when [A] and [B] are dissolved substances (M L^{-1}), and $m=0$ and $n>0$, then, $Eh=\Delta E^{\circ}+(0.0591/n)\log([B]^{b}/[A]^{a})$
4. when [A] and [B] are dissolved substances (M L^{-1}), and $m=>0$ and $n>0$, then, $Eh=\Delta E^{\circ}+(0.0591/n)\log([B]^{b}/[A]^{a})+([-0.0591m/n\ [pH]])$
5. when [A] and [B] are solid substances, and $m>0$ and $n>0$, then, $Eh=\Delta E^{\circ}+([-0.0591m/n\ [pH]])$
6. when [B] is a solid substance and [A] is a dissolved substance (M l^{-1}), and $m>0$ and $n=0$, then, $\log([A])=\Delta E^{\circ}+m\ [pH]$
7. when [B] is a solid substance and [A] is a dissolved substance (M l^{-1}), and $m>0$ and $n>0$, then, $Eh=\Delta G^{\circ}/(nF)+(0.0591/n)\log([A])+([-0.0591m/n\ [pH]])$.

The partial pressure of the gaseous reactants/ions (e.g., H, O, CO, CO_2, C_xH_y, etc.) alters $k_{observed}$, as $k_{observed}=k(P_p)^{xm}$ and $K_p=K(RP)^{cp}$, [21, 131].

The interactions between Eh, pH, partial pressure of (pH_2), and partial pressure of [O_2] (pO_2) are defined by the relationships [103]: (i) Hydrogen: $Eh=0.00–0.0591\ pH–0.0295\log(pH_2)$ [$2H^{+}+2e^{-}=H_2(g, aq)$], (ii) Oxygen: $Eh=1.228–0591\ pH+0.0147\log(pO_2)$ [$2H_2O=O_2(g, aq)+4H^{+}+4e^{-}$].

These relationships imply [10, 103, 104] that if ZVM is able to alter the Eh and pH of water, that the resultant remediation (e.g., Appendix 1.B) is both non-catalytic, and a natural consequence of an Eh, pH modification of pore water chemistry. This model assumes that the primary role of ZVM during the remediation process is to alter the water Eh and pH [10].

1.3.3 Galvanic Model

The presence of ZVM creates two primary products in water [103, 104]. They are e^{-} and H^{+}. Secondary products include H, H_2, O, O_2, O_2^{-}, O^{2-}, OH, OH^{-}, O_2H, O_2H^{-}, H_2O_2 [103, 104, 132]. The ZVM gradually degrades to produce ZVM ions [Fe^{n+}, Al^{3+}, Cu^{n+}] and associated ion adducts [103, 104, 132].

1.3.3.1 Diabatic Environment Remediation by ZVM injection into soil, or groundwater (<25 m depth), takes place in a diabatic environment where the temperature, T, is a function of atmospheric temperature [133, 134]. T varies during the day and seasonally over the year [133, 134]. Daily variations in T decrease with increasing depth [133]; daily variations of T are within the range <1 to >15°C; annual variations are within the range <1 to >50°C. Changing T will change the partial pressures of H_2 (and O_2) and one or more of pH, Eh, K, Q, $k_{observed}$ [103, 104, 131, 132]. Where the remediation reaction is reversible, and $E_a>0$, decreases in temperature may result in $k_d<k_{-d}$ and reversal of the remediation reaction (and vice versa). When Eh and pH are largely unaffected by changes in T, and ion removal is by precipitation (Appendix 1.B) then, a change in T of 1°C changes $\log([B]^{b}/[A]^{a})$ by $(R\ln[K])/(0.0591/n)$ [103]. Consideration of temperature variation is therefore a major variable when predicting the effectiveness of a groundwater remediation program.

1.3.3.1.1 Redox Trajectory Placement of n-ZVM in a diabatic groundwater environment results in a gradual change in Eh, pH over time [10, 17, 135] as the oxidation state of the Fe^0 increases (Fig. 1.1b–d). The redox trajectory is a function of Fe^0 particle size [10, 17, 135] (Fig. 1.1b and c), Fe^0:water ratio [10, 17] (Fig. 1.1b and c) and ZVM composition [10, 135] (Fig. 1.1d) [10, 135]. Daily variations in temperature [134] force an oscillation in both Eh and pH [10, 96, 135] (Fig. 1.1e and f), while maintaining a relatively constant hydrogen partial pressure (pH_2) (Fig. 1.1g). pH_2 can be independent of ZVM composition (Fig. 1.1g).

The general redox oscillation (Fig. 1.1e and f) is accompanied by a cyclic oscillation in EC [10, 135] (Fig. 1.1h), which reflects adjusting $Fe(OH)_x$, FeOOH, Fe_xO_y composition [10, 96, 135]. Each oscillation cycle commences with a large swing in EC, which dampens with time (Fig. 1.1h). These EC oscillations (Fig. 1.1h) reflect oscillations in Eh, pH, K, $\log(B]^{b}/[A]^{a})$ and are directly linked to cyclic changes in temperature (Fig. 1.1i and j).

1.3.3.2 Remediation Types Fe^0 remediation reactions fall into two basic groups: (i) irreversible, ZVM, or e^{-}, catalyzed reactions, or reaction sequences (Type A) (e.g., nitrate, PCE removal [10]), and (ii) reversible redox, or ZVM (oxide, hydroxide,

peroxide) substitution reactions (Type B) [10, 101–104]. Type A reactions are described by the Catalyst model, Redox model, and Galvanic model, while Type B reactions are described by the Redox model, Galvanic model, and Adsorption model.

1.3.3.2.1 Galvanic Type A Reactions Type A reactions require e^-, or H^+, or O_2 (e.g., electron shuttle and Fenton Reactions [10, 135]) to produce a product. They are favored by changes to the redox (Eh:pH) environment as [103]

$$\log\left(\frac{[B]^b}{[A]^a}\right) = Eh - \Delta E^\circ + \frac{[-0.0591m/n[pH]]}{0.0591/n} \tag{1.9}$$

Type A reactions are theoretically reversible, but in practice many are effectively irreversible (e.g., nitrate removal [10, 24–33, 129], TCE removal [10, 17, 54–57, 136]). For example [57], PCE (C_2Cl_4) degrades to C_2Cl_2 and TCE (C_2CH_3H). TCE degrades to DCE ($C_2Cl_2H_2$) and C_2ClH. DCE degrades to VC (C_2ClH_3), C_2H_2, and C_2H_4. VC degrades to C_2H_4. C_2Cl_2 degrades to C_2ClH, which then degrades to C_2H_2, which is then hydrogenated to C_2H_4. C_2H_2 and C_2H_4 are hydrogenated to C_2H_6 and C_xH_y [94, 96]. E_a for nitrate removal is in the range 21–46 kJ mol^{-1}[6, 30]. E_a for PCE/TCE/chlorinated hydrocarbon removal is in the range 9.8–80 kJ mol^{-1}[11, 136]. Since $\Delta E^\circ = -RT \ln[K]$ and $\ln[K] = \Delta E^\circ/RT$ [103, 104], it follows that increasing temperature, while maintaining a constant Eh and pH (when $\Delta E^\circ > 0$), will decrease the equilibrium ratio ($[B]^b/[A]^a$). It will also increase the reaction rate ($k_{observed}$) (Eq. 1.4).

From Equation 1.3, it follows that the principal controls on a Type A remediation program are ZVM particle size, particle type, mass ratio of pollutant:injected ZVM, and the injected ZVM:water/gas slurry concentration (g l) [137]. A relatively small reduction in particle size (from >1000 to 50–300 nm) can allow a major reduction in the amount of ZVM required to remove greater than 99% of the TCE in the groundwater (Fig. 1.1b and c).

From Equation 1.9, it follows that remediation is enhanced by increasing the availability of e^- by increasing the O_2 saturation of the pore water [138, 2, 139–141], while maintaining a constant, or decreasing, pH, and/or decreasing the aquifer pH by injection of CO_2 [94, 96, 2, 139–141] or addition of acidic components, for example, $FeCl_y$, while maintaining a constant or decreasing Eh [[10], [21], [95], [103], [142]]. It also follows (from Eqs. 1.3–1.5) that increasing the groundwater temperature by water injection, steam injection, or gas injection may reduce the time and amount of n-ZVM required to achieve a specific level of remediation from, for example, 100 days, to between <1 day and >50 days.

1.3.3.2.1.1 GALVANIC TYPE A REACTIONS: IMPACT OF OXYGENATION In oxygenated water, n-Fe^0 behaves as an iron–oxygen redox cell [138], where the overall reaction is $Fe^0 + 0.5O_2 + H_2O = Fe(OH)_2$ [Cathode {+} reaction : $0.5O_2 + H_2O + 2e^- = 2OH^-$; Anode [−] reaction: $Fe^0 + 2OH^- = Fe(OH)_2 + 2e^-$; pH = <10.53]. $Fe^0 = Fe^{2+} + 2e^-$; $Fe^{2+} + 2OH^- = Fe(OH)_2$ when the Fe^{2+} concentration is greater than (log $(Fe^{2+}) = 13.29 - 2pH$ [103]. At a pH > 10.53, $FeOOH^- + H^+ = Fe(OH)_2$ when the $FeOOH^-$ concentration is greater than (log $(FeOOH^-) = -18.30 - pH$ [103]. The relative stability of the Fe^{2+} and $FeOOH^-$ ions is provided by the molar relationship $\log[FeOOH^-/Fe^{2+}] = -31.58 + 3pH$ [103]. The addition of oxygen into the iron–air cell modifies the standard redox cell used to produce $Fe(OH)_2$ from: (i) $Fe + 2H_2O = Fe(OH)_2 + 2H^+ + 2e^-$ (Eh for phase boundary is [103]: $Eh = -0.047 - 0.0591$ pH) to; (ii) $Fe^0 + 0.5O_2 + H_2O = Fe(OH)_2$ (Eh for phase boundary is [103]: $Eh = -1.29 - 0.0591$ pH). The net effect is an increase in the availability of e^-, and an increase in the associated remediation rates. At any given time, the concentration of e^- in the water is [103]: e^- [M l^{-1}] = $10^{((Eh\ (water) + 1.125)/0.0295) - pH\ (water))}$. Magnetised n-$Fe^0$ will preferentially attract O_2 (e.g., $Fe^0 + O_2 + 2H^+ = Fe^{2+} + H_2O_2$; $Fe^{2+} + H_2O_2 = Fe^{3+} + 2HO + e^-$) [2]. Chlorinated organics are removed from oxygenated water by an electron shuttle mechanism using Fe^0 or Al^0. A simple shuttle mechanism, where e^- acts as a catalyst [130], is provided as $H_zC_xCl_y + e^- + H = [H_{z+1}C_xCl_{y-1}] + Cl + e^-$. The electron shuttle model predicts that increasing the availability of e^- by oxygenation, or another mechanism, will increase the remediation rate. Experiments have established that oxygenation increases the rate of remediation reaction (for As removal) by greater than 4 fold (over a 60-min period) but does not necessarily reduce Eh [139–141], through the reversible equilibrium reactions $Fe^0 + 2H_2O = Fe^{2+} + H_2 + 2OH^-$; $Fe^{2+} + H + e^- = FeH^+$; $FeH^+ + O = FeOH^+$; $Fe^0 + 2H_2O + O_2 = 2Fe^{2+} + 4OH^-$; $2Fe^{2+} + nOH^- = Fe(OH)_n$, etc. (Fig. 1.2). Effective anion removal (e.g., As) is enhanced in an acidic environment [101–104, 2, 139–141]. This can be achieved by acidifying the water by CO_2 injection [139–141] or acid injection [2, 139–141], prior to n-Fe^0 injection, and oxidation [139–141]. e^- generation through a strategy of cyclic n-Fe^0 oxidation and reduction appears to be effective over greater than 4000 redox cycles [138].

1.3.3.2.2 Galvanic Type B Reactions Type B remediation reactions occur when (i) the interaction of T, Eh, pH changes resulting from the presence of ZVM, results in a change in K, which allows pollutant ions to be precipitated as oxides, peroxides, hydroxides, sulfides, carbonates, etc (e.g., Appendix 1.A), and (ii) when the Fe^0 corrodes to one or more of n-FeH^{n+}, n-$Fe(OH)_x$, n-FeOOH, n-Fe-$[O_xH_y]^{(n+/-)}$) (Fig. 1.2). Subsequent Fe ion substitution/adsorption (or Fe ion adduct formation) of cations and

anions (Fig. 1.3) results in pollutant cation/anion removal from the water, with precipitation within a n-Fe-[O_xH_y] structure–Adsorption Model [101, 102].

At any specific (constant) pH (e.g., pH = 7), both cations and anions are removed [143]. The total amount of cations removed may increase, or decrease, with changing temperature [144], and may be a function of both pollutant concentration, and the concentration of other anions (e.g., humic acids) within the groundwater [144]. Anion and cation removal increases with time [145], and the ratio of cations:anions removed by incorporation/substitution varies with the pollutant ion adduct:Fe^{n+} ratio in the water [144]. Fe(II) ions (and other cations) hydrolize on the surface of FeOOH particles [146].

1.3.3.2.2.1 GALVANIC TYPE B REACTIONS: POM AND HPOM PRODUCTS Polyoxometalates (POMs) (Fig. 1.2) are self-assembly accretionary molecules that take the form of a sandwich composed of a central core fragment $Fe^{II}_n\ Fe^{III}_mO_z.(H_2O)_y$ surrounded by external fragments of $Fe^{II}_n\ Fe^{III}_mO_z.H_2O_y$ linked by two distinct edge sharing dimeric clusters of $(Fe(OH)_2$ [147, 148]. The formation of POMs greatly increases the rate of n-ZVM water remediation by serving as an electron shuttle and ion chelating agent [149]. A POM (Fig. 1.2) may potentially remove (Fig. 1.3) greater than 10 g Cation g^{-1} n-Fe^0. The associated by-product Type A reactions, involving e^- catalysis, may remove greater than 1 g pollutant g^{-1} n-Fe^0.

Heteropolyoxometallates (HPOM) are derived from metal cages of the form $(MO_n)_x$, which incorporate anion templates of the form (AO_x^{n-}) [150]. However, their pentagonal building blocks form around a pentagonal bipyramidal core (MO_n), which can be hydrated [150]. A typical HPOM nucleates around a cluster of 2 Fe ions (oxidation state 2^+ or 3^+ or 4^+). They seed a linkage, which allows clusters of pentagonal, or another structural form, of $M(1)O_n$ to accrete [150]. In saline water, the monomer may take the form $[K_{8+x}Na_{9+y}H_{29+z}[H_{34}M(1)_{119}M(2)_8Fe_2O_{420}(H_2O)_{34+n}]]^{(8-x-y-z)-}$; the diamer may take the form $[K_{16+x}Na_{1\ 9+y}H_{57+z}[H_{34}M(1)_{119}M(2)_8Fe_2O_{420}(H_2O)_{74+n}]]^{(16-x-y-z)-}$ [150]. M(1) and M(2) are different metal cations incorporated in the HPOM from the water. An individual HPOM molecule may have a size of less than 3 nm [150]. HPOM formation is slow and conversion of 4% of the n-Fe^0 to HPOM may take greater than 4 weeks [150]. However, they are highly effective remediation agents [149] with a potential absorption capacity of greater than 100 g pollutant cation g^{-1} n-Fe [150]. Injection of 100 kg n-Fe^0 into groundwater can potentially result in greater than 400 kg of pollutant cations being removed in HPOM structures over a 4-week period.

1.3.3.2.2.2 GALVANIC TYPE B REACTIONS: IMPACT OF HYDROGEN In poorly oxygenated water, the n-Fe^0 gradually corrodes (Appendix 1.C, Fig. 1.2) to form a corrosion zone of Fe-hydroxides and peroxides at the n-Fe^0–water interface [10]. The interface acts as a hydrogen electrode (cathode) and the Fe^0 acts as a current electrode (anode). During remediation, Fe/Cu acts as a cathode to an Al anode. The Cu acts as a cathode to a Fe anode [151–154]. The basic process involves charge transfer (and OH ion formation) at the ZVM–water interface and includes electron transfer via conduction, electron insertion into active sites, and conduction by hopping through electron-deficient lattice sites within the active material [151].

In a diabatic environment, the perpetual oscillation and change in temperature (Fig. 1.1i and j), results in a perpetual oscillation between forward and backward reactions (Fig. 1.2). This oscillation allows the hydrides/hydroxides/peroxides/oxides (Fig. 1.2) to be used as stores of protons (H^+) and electrons (e^-) [151–154], which can be accessed for Type A remediation reactions. All changes that increase the oxidation number of the ZVM ion adducts, effectively result in electron storage (charging) occurring and vice versa [151] (Fig. 1.2). Ions (aqueous or solid) that contain an oxidation number greater than the stoichiometric charge are overcharged [151] (Fig. 1.2).

1.3.3.2.2.3 GALVANIC TYPE B REACTIONS: DISCHARGE During discharge, electrons flow from the current electrode (Fe^0 particles [$Fe^0 = Fe^{n+} + ne^-$] and other ZVM and ZVM adducts (Figs. 1.2 and 1.3, Appendix 1.C)), through the hydroxides, peroxides (Fig. 1.2)–charge transfer sites [e.g., $FeOOH + H_2O + e^- = Fe(OH)_3 + e^-$; $FeOOH + OH^- + H^+ + e^- = Fe(OH)_3 + e^-$] to the hydrogen electrode (Cu^0 particles) [151]. Hydrogen generation occurs at the particles, which act as a hydrogen electrode [$2H_2O + 2e^- = 2H^+ + 2OH^- + 2e^-$; $2H_2O + 2e^- = H_2 + 2OH^-$].

1.3.3.2.2.4 GALVANIC TYPE B REACTIONS: RECHARGE During recharge, the electron flow is reversed [151] and oxygen forms at the cathode as a by-product of electron generation [cathode–electron generation: $4OH^- = O_2\ (g) + 2H_2O + 4e^-$; hydroxide reduction to peroxide in the charge transfer sites: $Fe(OH)_3 = FeOOH + H_2O + e^-$; Fe ion reduction to Fe^0] [151].

1.3.3.2.2.5 GALVANIC TYPE B REACTIONS: GAS EVOLUTION During recharge, oxygen accumulates in the charge transfer sites [151]. During discharge, hydrogen accumulates in the charge transfer sites [151]. Both gases show very different morphologies at the ZVM–water interface [10]. Oxygen bubbles tend to form in, and are commonly encased by, the cathodic particles (e.g., Cu) [10], and form rapidly after a ZVM mixture (Fe+Cu, Fe+Cu+Al (Fig. 1.4a–d)) is placed in the reactor. The initial corrosion reactions are recharge reactions forming FeOOH. The FeOOH forms active charge sites. The formation of hydrogen gases initially results in the adsorption of the O_2 gas bubbles, with no hydrogen gas discharge (i.e., $2H_2 + O_2 = 2H_2O + \text{heat}$) [151].

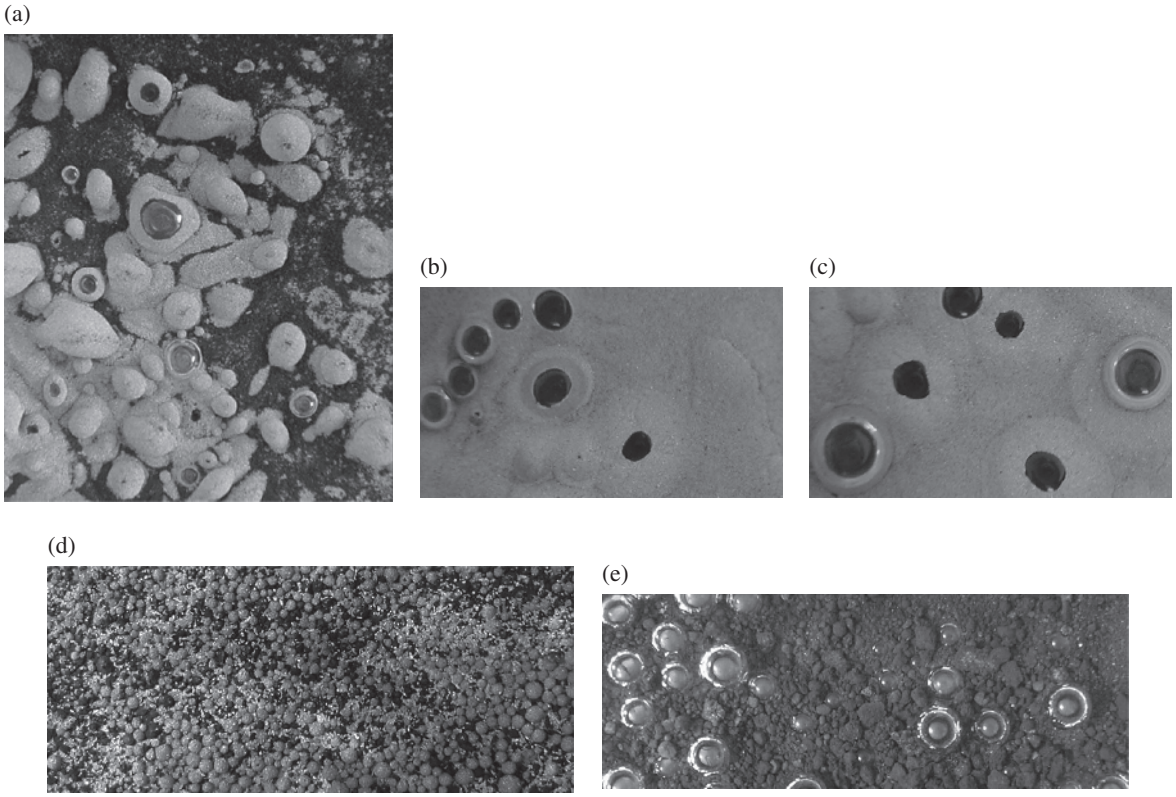

FIGURE 1.4 Morphology of common gas bubbles associated with n-Fe^0 (Nanofer Star (supplied by nanoiron s.r.o.; www.nanoiron.cz), 50 nm, BET = 20m^2 g^{-1}; mixed with n-Al^0 and n-Cu^0) (a) Oxygen bubbles encased by Cu^0 on the surface of n-Fe^0 [5 g n-Fe^0 + 5 g n-Cu^0 + 0.25 l saline H_2O [Eh = 0.095 V; pH = 7.01; EC = 1.993 mS cm^{-1}; T = 12.8 C – gas composition checked using TCD GC]]. (b) O_2 gas venting where n-Al^0 rests on top of n-Fe^0. The O_2 gas bubbles are encased by n-Cu^0. [5 g n-Fe^0 + 5 g n-Cu^0 + 5 g n-Al^0 + 0.25 l saline H_2O [Eh = 0.073 V; pH = 7.00; EC = 1.981 mS cm^{-1}; T = 12.9 C– gas composition checked using TCD GC]]. (c) O_2 gas venting where n-Al^0 rests on top of n-Fe^0. [5 g n-Fe^0 + 5 g n-Cu^0 + 5 g n-Al^0 + 0.25 l saline H_2O [Eh = 0.073 V; pH = 7.00; EC = 1.981 mS cm^{-1}; T = 12.9 C– gas composition checked using TCD GC]]. (d) O_2 filled spheres of n-Cu^0 developing on the n-Fe^0 – water interface, 5 min after loading into a reactor. [40% n-Fe^0 + 20% n-Cu^0 + 40% n-Al^0]. (e) H_2 gas bubbles developing on the ZVM-water interface (Fig. 1.4d), 3 weeks after loading [H_2 composition verified by TCD GC]. Part of the n-Fe^0 has been corroded to form agglomerated FeOOH and Fe_3O_4 nodules or clods (0.5–4 mm in diameter). Some of the nodules are coated with n-Cu^0. Each nodule forms an accreting galvanic cell (Fig. 1.2) with an anodic core (e.g., n-Fe^0, n-Al^0, $Fe(OH)_2$) and a cathodic exterior (e.g., n-Cu^0, n-FeOOH, n-Fe_3O_4). Individual gas bubbles are 3–6 mm in diameter.

After the FeOOH corrosion products (Fig. 1.2) reach a critical mass, the ZVM switches from operating in a net recharge mode, to operation in a net discharge mode. During this phase, distinctive hydrogen gas bubbles form on the ZVM/FeOOH surface (Fig. 1.4e). Unlike the O_2 bubbles, H_2 bubbles are not associated with a specific cathodic ZVM, but instead form on the surface (and in) active charge transfer sites (e.g., FeOOH, Fe_3O_4 (Fig. 1.4e)).

1.3.3.2.2.6 GALVANIC TYPE B REACTIONS: HYDROGEN EVOLUTION The amount of hydrogen generated is a function of ZVM composition, water composition, and operating conditions (pressure, temperature) [155–157]. The maximum hydrogen production occurs when the n-ZVM is reduced to the ZVM oxide (Fig. 1.2). For example, $xZVM + yH_2O = ZVM_xO_y + yH_2$. For the reaction $3Fe + 4H_2O = Fe_3O_4 + 4H_2$ (Figs. 1.2 and 1.4e), 167 g n-Fe^0 (50 nm) + 72 g H_2O = Fe_3O_4 + 8 g H_2 (89.64 l) [158]. This process can be undertaken over a short time period using n-Fe^0 (50 nm). Increasing the temperature of a water:n-Fe^0 mixture from <20 to 350°C over a 90-min period, in a sealed diffusion reactor, will result in a H_2 yield of about 450–540 m^3 H_2 t^{-1} n-Fe^0, and a gas pressure of greater than 5 MPa [159]. Cooling the reactor to 20°C provides a deliverable H_2 gas at less than 3 MPa [159]. Reduction of the Fe_3O_4 to Fe^0 allows the cycle to be repeated (e.g., $Fe_3O_4 + 4CO = 3Fe^0 + 4CO_2$; $Fe_3O_4 + 4H_2 = 3Fe^0 + 4H_2O$) [159, 160]. In a confined diffusion reactor, the general reactions (Fig. 1.2), result (at T = <50°C) in low levels of pressurized H_2 gas evolution as the Fe^0 oscillates between charged (Fe^{III}) and discharged (Fe^{II}) states [155–157].

The oscillating combination of H^+ and e^- generation from the cathodic sites during recharge and discharge [151, 153] creates the driving force for chlorinated hydrocarbon (and other Type A) remediation [161].

1.4 REMEDIATION MARKET

Contaminated sites (soils and groundwater) vary in size from <100 m^2 to >10 km^2. The number of contaminated sites, which could benefit from n-ZVM treatment, is estimated at 350,000–400,000 in Europe, 235,000–355,000 in the United States [136, 162]. There are probably a similar number of contaminated sites in Canada, S. America, China, Russia, India, The Middle East, Asia, Australia, and Africa. To date, only a few sites have been treated using n-ZVM.

1.4.1 Remediation Costs

A typical PCE/TCE/DCE groundwater remediation costs around \$200–\$700 kg n-Fe^0 used [137, 162], and utilizes less than 1–280 *t* n-Fe^0 for each t PCE/TCE/DCE in the soil/aquifer [17, 137]. The cost comprises a n-Fe^0 cost (e.g., \$30–\$100 kg^{-1}) + injection/infiltration + monitoring costs. Since the radius of influence of an injection well/infiltration point source is typically less than 40 m [22, 23], reducing the n-Fe^0 cost will not necessarily reduce the costs associated with injection/infiltration and monitoring. Remediation adds value by either allowing the land to be rehabilitated, for industrial, domestic, or agricultural applications, or by allowing the water to be used for municipal, industrial or agricultural purposes. The sustainable remediation cost is a function of the overall value added by the remediation.

1.4.1.1 Reduction of Type A Remediation Costs Type A remediation costs are reduced by (i) reducing both particle size and the amount of ZVM injected (Eq. 1.3). Compare with Figures 1.1b, c, which both achieved greater than 99% removal of 25–88 mg TCE l^{-1} H_2O [17]; (ii) increasing groundwater temperature [130] (Eq. 1.4, and/or oxygen levels [138, 2, 139–141], and/or increasing groundwater acidity [10, 103, 104, 135, 142] (Eqs. 1.4 and 1.9), in order to both accelerate the remediation and reduce the overall amount of n-Fe^0 required. The catalytic model assumes that 1 mol n-Fe^0 can only generate 2 or 3 mol e^- (Appendix 1.C) and that increasing particle size will increase the active life of the n-Fe^0 [163]. The galvanic model assumes that the perpetual oscillations [10] within the groundwater will allow a substantially greater amount of e^- and H^+ to be formed using a cyclic process. That is,

1. $H_2O^- + Fe^{2+} = FeH^{2+} + OH^-$; $H + Fe^{2+} = FeH^{2+}$;
2. $H_3O^+ + FeH^{2+} = H_2O + H_2 + Fe^{3+}$; $H_2 = 2H^+ + 2e^-$; $H^+ + e^- = H$
3. $H + Fe^{3+} = H^+ + Fe^{2+}$ [132]

Fresh oxygen contained in recharge water entering the remediation zone will be initially removed [132] as $O_2 + Fe^{2+} = O_2^- + Fe^{3+}$; $O_2 + FeOH^+ = O_2^- + FeOH^{2+}$; $O_2 + Fe(OH)_2 = O_2^- + Fe(OH)_2^+$, $O_2 + Fe(OH)_3^- = O_2^- + Fe(OH)_3$, etc. The O_2^- interacts with $FeO_xH_y^{n+/-}$, H_2O, O_2H, OH and H to form O^-, O^{2-}, O_2 O_2H, OH, H_2O_2 and $FeO_xH_y^{n+/-}$ [132]. This allows recharge of oxygenated water (from surface precipitation and subsurface flow) to provide a natural drive for the galvanic cell.

1.4.1.1.1 Reduction of Type A Remediation Costs: Catalytic Model The cathodic model focuses on reducing particle size and increasing temperature to increase remediation rates and reduce the amount of ZVM required. Figures 1.1b, c demonstrate that the same degree of TCE remediation can be achieved using 3.9 kg n-Fe^0 (>1000 nm) m^3 soil and 0.009 kg n-Fe^0 (50–300 nm) m^3 soil. The total n-Fe^0 surface area in Figure 1.1b is about 20 times greater than the n-Fe^0 surface area in Figure 1.1c. Brownfield development land may economically sustain a remediation cost of \$3–\$6 MM/acre (i.e., \$75–\$1500 m^3 soil/aquifer), depending on location and final use. Comparative costs for surface reactor treatment of industrial water and agricultural water to remove chlorinated hydrocarbons and nitrates using ZVM in fixed/packed bed reactors are in the order of \$0.03 m^{-3} H_2O for greater than 90% removal [10, 13].

1.4.1.1.2 Reduction of Type A Remediation Costs: Galvanic Model The galvanic model indicates that the concentration of Fe^{2+}, $FeO_xH_y^{n+/-}$ ions and the presence of a controlled instability in the groundwater following ZVM injection (e.g., temperature variation, oxygen variation, acidification) controls the rate of Type A remediation. These factors facilitate remediation through electron shuttle reactions [164–166]. A galvanic cell of this type (Fig. 1.2) can be sustained through greater than 200,000 cycles/oscillations [151]. Application of this model to brownfield site remediation will (i) reduce the amount of n-Fe^0 required to achieve a specific level of remediation within a specific timeframe; and (ii) reduce the remediation time required using a specific amount of n-Fe^0. Remediation time frames for TCE removal can be potentially reduced from >1 year to <1 week.

1.4.1.2 Reduction of Type B Remediation Costs Type B remediation (Appendix 1.B, Fig. 1.3) can be undertaken using n-ZVM or ZVM corrosion products (Fig. 1.2). The remediation occurs over a long timeframe (days to years), which is controlled by the ZVM concentration, Eh, pH, and ion type. The amount of contaminant removed increases with time, and is typically in the range less than 0.01–0.3 g contaminant g^{-1} n-Fe^0. The galvanic model allows the timeframe required to remove specific pollutants (Appendix 1.B), and the total amount of pollutant removed to be reduced by controlling the Eh, pH environment, and ZVM composition with time. Remediation rates during active galvanic management can potentially exceed 1 g pollutant g^{-1} n-Fe^0. Active subsurface Eh:pH management using the galvanic model may be able to reduce the treatment costs to less than \$2 MM/acre (i.e., \$5–\$150 m^3 soil/aquifer).

1.5 CONCLUSIONS

Groundwater remediation (Type A and B) using ZVM is typically undertaken by ZVM infiltration, or pneumatic injection of ZVM [17, 137] using a passive process of injection followed by monitoring over a number of years. This approach, which assumes that the catalytic model applies, provides little, or no, effective day to day control over the rate of remediation. The observation that bimetallic ZVM (e.g., n-Fe^0 + one or more metals where $E° < E°\ Fe^{II}$ (Appendix 1.C)) shows increased reactivity (and delayed rates of Fe^0 oxidation) when compared with n-Fe^0 [179] is consistent with the galvanic model. The close proximity of the cathodic and anodic species coupled with diabatic oscillations results in continual oscillating reduction and oxidation of the bi-metal species. In mono n-Fe^0 the initial oxidation (formation of Fe-$(OH)_2$) (associated with galvanic oscillation between Fe^{II} and Fe^{III} (Appendix 1.C)) results initially in exponential particle growth [179]. This switches to logarithmic particle growth as the cathodic species $Fe(OH)_3$, FeOOH, and Fe_xO_y start to form [179]. The associated by-products, which react [10] to remove contaminants, are [e.g., 103] e^-, H, H^+, OH, OH^-, O_2H, O_2H^-, H_2O_2, O, O^-, O_2^-, and O^{2-}. Particle growth and agglomeration is rapid with 50 nm particles forming agglomerations of greater than 1 mm within 21 days (e.g., Fig. 1.4e, see also [10]). n-FeO_xH_y expulsion with (H_2, O_2) gas bubbles results in a rapid and effective dispersion of colloidal Fe^{II}–Fe^{III} galvanic cells throughout the water column. These grow with time (Figs. 1.2 and 1.3) to form colloidal particles greater than 1 mm in diameter, which settle on the ZVM–water interface [10]. The n-colloid clouds in the water within the diffusion environment tend to be monospecific, color coordinated (e.g., white = $Fe(OH)_2$; yellow/orange = $Fe(OH)_3$; blue-green = green rust; dark-red brown/black = FeOOH; oxygenated blood red = Fe_2O_3; grey/black = Fe_3O_4), and indicate the galvanic charge status within the reaction environment (Fig. 1.2). The dominant colloid species changes with Eh, pH, and charge status of the water. The accreting growing colloidal particles, which can grow from 50 nm to greater than 5 mm, obtain buoyancy from H and O, which are present on the active sites.

An understanding of the corrosion of n-Fe^0 in the remediation environment and the controls that allow the net reaction directions (Fig. 1.1e–h) to be switched between recharge (formation of Fe^{III} ion adducts) and discharge (formation of Fe^{II} ion adducts) (Figs. 1.2 and 1.3) is an essential prerequisite to understanding how to reduce the cost and increase the efficiency of the remediation program.

The galvanic model requires active post-injection management of the groundwater Eh, pH temperature, and oxygenation levels. It has the potential to allow 15–100 nm Fe^0, Cu^0, Al^0 (typically spherical/blocky) particles with a surface area of 10–80 $m^2\ g^{-1}$, and costing \$20,000–\$850,000 t^{-1}, to be restructured and replaced by specific galvanic components (5–80 nm) with a layered structure [(e.g., $Fe(OH)_x$, FeOOH, etc. (Fig. 1.2)) and a surface area of <100 to >30,000 $m^2\ g^{-1}$ Fe^0, costing around \$300–\$15,000 t^{-1}]. The net effect of this restructuring is to reduce the amount of n-Fe^0 required, the rate of remediation, the time frame for remediation, and the overall cost of the remediation while increasing the amount of pollutant removed g^{-1} n-Fe^0.

APPENDIX 1.A LIST OF ABBREVIATIONS AND EQUATION SYMBOLS

1. *a*, *b*, *d*, *e*, *m*, *n*, and *p* are constants which are determined experimentally. In a simple non-catalytic example where $b = 0$, m = the reaction order [130]. The reaction order is calculated as m + n + p [130].
2. A' = a constant (0.509 $dm^{1.5}\ mol^{-0.5}$ at 298K);
3. A_f = pre-exponential factor [$E_{a(sa)}$ & $A_{(sa)}$ = normalized for p_m and a_s; $E_{a(observed)}$ & $A_{(observed)} = E_a$ and A_f calculated without correction or normalization for p_m and a_s.
4. $a_{s(t=n)}$ = ZVM surface area(m^2 gm) at time t. $a_{s(t=n)}$ decreases with increasing time as the ZVM surfaces become oxidized;
5. B' = a constant; a = radius of the ion;
6. C_a = catalyst (e.g., ZVM);
7. $C_{t=n}$ = contaminant concentration at time, t = n (seconds) [mg l^{-1}, M l^{-1}];

8. $C_{t=0}$ = initial contaminant concentration at $t = 0$ [mg l^{-1}, M l^{-1}];
9. c_i = concentration (mol dm^{-3}; mol l^{-1}) of the ith ion of charge, z_i.
10. cp = moles gaseous reactants-moles gaseous products;
11. $D_{\{A[ZVM]\}}$ = diffusion coefficient = $k_B T / \pi\beta\eta\, r_s$;
12. D_f = Driving force, Pa (1 m head = 10,000 Pa);
13. E_a = Activation energy (kJ Mol^{-1});
14. F = Faraday constant;
15. H = Planck's constant;
16. I = ionic strength of the water = $0.5\ \Sigma\ c_i Z_i^2$;
17. $\log(\gamma_A) = -A' z_A^2\ I^{0.5}$ (lower ionic strengths);
18. $\log(\gamma_{A)} = -A' z_A^2\ I^{0.5}/(1+B'a\ I^{0.5})$ (higher ionic strengths);
19. $\log(k_{observed}/k_o) = 1.018\ z_A\ z_B\ I^{0.5}$;
20. k_B = Boltzmann's constant;
21. k_o = the rate coefficient at zero ionic strength = $k_r K_{AB}$;
22. $k_{observed}$ = observed contaminant removal rate constant [proportion removed s^{-1}]; $k_{observed}$ can also be expressed as mg removed s^{-1}, or [moles removed mole reactant^{-1} s^{-1}], or another suitable set of units;
23. k_p = permeability, $m^3\ m^{-2}\ s^{-1}\ Pa^{-1}$;
24. k_{sa} = reaction rate constant which has been normalized for ZVM surface area and ZVM concentration in the water;
25. K, K_{AB} = Equilibrium constant;
26. K_p = equilibrium constant adjusted for pressure;
27. $K^{\ddagger}\ (\gamma_A\ \gamma_{ZVM}/\gamma_{\{A[ZVM]\}}) = \exp(-\Delta G^{\ddagger}/RT)$ and $RT(\mathrm{Ln}\ (K^{\ddagger}\ (\gamma_A\ \gamma_{ZVM}/\gamma_{\{A[ZVM]\}})) = -\Delta G^{\ddagger}$;
28. n = number of electrons transferred;
29. P = pressure;
30. P_p = reactant partial pressure;
31. p_m = mass concentration of ZVM at t (g l^{-1}). p_m decreases as ZVM ions are removed with the product water and as ZVM is replaced with ZVM-hydroxides, peroxides, oxides, carbonates, sulphates, sulphides, etc.;
32. Q = reaction quotient;
33. Q_{fr} = flow rate, m^3 hr;
34. R = gas constant;
35. $r_{\{A[ZVM]\}}$ = encounter radius (nm) of the reactant [A]: ZVM interaction;
36. r_s = hydrodynamic radius (nm) of the diffusing species;
37. SV = space velocity, $m^3\ hr^{-1}\ t^{-1}$ ZVM;
38. SWZ = stored water to ZVM ratio in the reaction environment, $m^3\ H_2O\ t^{-1}$ ZVM;
39. S_w = Volume of water contained in the reaction environment, m^3;
40. T = Temperature, K;
41. t (time) can be expressed in seconds, minutes, hours, days;
42. W_{zvm} = weight (t) of ZVM in the reaction environment;
43. Xm = number of moles of the gaseous reactant;
44. z_A = charge number of ion species;
45. z_B = charge number of ion species, B;
46. ZVM = zero valent metal;
47. H = viscosity;
48. B = a constant (continuum solvent, $\beta = 6$; molecular diffusion, $\beta = 4$);
49. K = transmission coefficient (e.g., 1.0);
50. ΔE^o = standard potential for the reaction; $\Delta E = Eh$;
51. $\Delta G^{\ddagger}$ = overall Gibbs free energy of activation = $\Delta G^o_{\{A[ZVM]\}} + \Delta G^*$;
52. ΔG^o = standard Gibbs free energy for a reaction;

53. $\Delta G^{o}_{\{A[ZVM]\}}$ = free energy change on forming the encounter pair;
54. ΔG^{*} = free energy of activation from the encounter pair;
55. $\Delta G = \Delta H - T\,\Delta S$;
56. ΔH = heat of reaction;
57. ΔS = entropy;

APPENDIX 1.B IONS (OXIDES, HYDRIDES, PEROXIDES, AND HYDROXIDES) REMOVED BY PRECIPITATION DUE TO THE ALTERATION OF Eh AND pH IN GROUNDWATER BY ZVM

Data Sources: [10, 103, 104, 167–175]

In the simplest case, n-ZVM addition leaves pH effectively unaltered (e.g., Fig. 1.1c).

Eh prior to addition of n-ZVM = Eh [103, 104, 131] = $\Delta E^{o} + (0.0591/n)\log([B]^{b}/[A]^{a})_{t=0}$. For an example contaminant removal reaction,

$$Cd^{2+} + H_2 = Cd(s) + 2H^{+}$$

(the half reactions are $Cd^{2+} + 2e^{-} = Cd^{0}$ and $H_2 = 2H^{+} + 2e^{-}$; see Appendix 1.C); $K = Q = [H^{+}]^2/([Cd^{2+}]P_{H2}) = B^{b}/A^{a}$ [131]. After n-ZVM addition, at time $t = m$, the Eh changes (Fig. 1.1b–d) result in a new equilibria, where the new $\log([B]^{b}/[A]^{a})_{t=m} = (Eh - \Delta E^{o})/(0.0591/n)$; ΔE^{o} is corrected to the actual groundwater temperature. In this example, if the groundwater at t = 0 contains a 0.001 M Cd^{2+} l^{-1} and an Eh of 0.13 V (Fig. 1.1c), then Eh = 0.13 = ΔE^{o} (–0.4 V—Appendix 1.B) + 0.0591/2 log Q; that is, log Q = 18; if –log (H^{+}) = pH [103, 131], then for pH = 6.5, at t = 0, $P_{H2} = 10^{-22}$. Changing the Eh to –0.2 V (Fig. 1.1c) after 1 month, while maintaining a pH of 6.5, changes log Q to 6.7. The Cd^{2+} concentration in the water at time, t = 1 month, is therefore a function of P_{H2} in the groundwater resulting from the presence of n-Fe^{0} (Fig. 1.4e). Increasing P_{H2} to 10^{-10} could achieve the observed Eh (–0.2 V) while leaving the Cd^{2+} concentration unchanged. Increasing P_{H2} to 10^{-8} reduces the Cd^{2+} concentration in water to 0.00001 M Cd^{2+} l^{-1} from 0.001 M Cd^{2+} l^{-1}; that is, the effectiveness of the n-Fe^{0} treatment program for any specific Eh and pH, where the product is a zero valent metal (Appendix 1.B), is maximized by increasing the H_2 partial pressure. The alternative remediation strategy of using O_2 injection to oxidize cations (e.g., $Cd^{2+} + 0.5O_2 + H_2O = Cd(OH)_2$, where $0.5O_2 + H_2O + 2e^{-} = 2OH^{-}$; $Cd^{2+} + 2OH^{-} = Cd(OH_2)$, and $H_2 = 2H^{+} + 2e^{-}$) effectively changes Q to $Q = [H^{+}]^2/([Cd^{2+}]\,P_{H2}P_{O2})$, and ΔE^{o} to 0.4 V [177]. This alternative strategy uses the n-Fe^{0} to control the groundwater pH (i.e., H^{+} and P_{H2}) and the P_{O2} associated with O_2 injection to control the rate and degree of remediation [139–141]. For example, if at t = 0, Eh = 0.13 V, pH = 6.5, and the water contains 0.001 M Cd^{2+} l^{-1} and $P_{H2} = 10^{-22}$, $P_{O2} = 0$, then instigation of an oxygen injection scheme following n-Fe^{0} injection into the groundwater, while maintaining a constant Eh and pH, will result in both P_{H2} and P_{O2} increasing [e.g., [139–141]]. Once P_{H2} and P_{O2} have exceeded a critical level (e.g., 10^{-11}), any subsequent increases in partial pressure will be compensated for by either decreases in Eh, or the removal of Cd^{2+} as $Cd(OH)_2$. Increasing P_{H2} and P_{O2} to 10^{-9}, will reduce the molar concentration of Cd^{2+} to 0.0000001 M Cd^{2+} l^{-1} (i.e., 0.146 g $Cd(OH)_2$ l^{-1} H_2O will have been precipitated into the ZVM bed). This simple example has been used to demonstrate how a traditional ZVM remediation program [e.g., [17]] can be modified using the galvanic model [138, 2, 139–141] to both accelerate and control the rate of remediation. Once the bulk of the cations have been converted to oxides/hydroxides/peroxides, the diabatic galvanic model (Figs. 1.2 and 1.3) controls the rate of remediation.

Contaminant Ion/Ion Adduct	Potentially precipitated by ZVM as
Ac^{3+}, $AcOH^{2+}$, $Ac(OH)_2^{+}$	$Ac(OH)_3$, AcOOH
Ag^{n+}, AgO^{+}, AgO^{-}, AgOH, $AgOH_2^{-}$, $AgCl_2^{-}$	Ag, AgCl, AgOH, Ag_2O, Ag_2O_2, Ag_2O_3
Al^{n+}, $HAlO_2$, AlO_2^{-}, $AlOH^{2+}$, AlOH3, $Al(OH)_2^{+}$, $Al(OH)_4^{-}$	$Al(OH)_3$, AlOOH, Al_2O_3
Am^{n+}, $AmOH^{2+}$, AmO_2^{+}, $Am(OH)_2^{+}$	$Am(OH)_3$, $Am(OH)_4$, AmO_2
AsH_3, $HAsO_2$, AsO^{+}, H_3AsO_4, $H_2AsO_4^{-}$, $HAsO_4^{2-}$, AsO_2^{-}, AsO_4^{3-}	As, AsO_3
Au^{n+}, H_2AuO_3, $H_2AuO_3^{-}$, $HAuO_2^{2-}$	Au, $Au(OH)_3$, AuOOH, AuO_2
Ba^{2+}, $BaOH^{+}$	$Ba(OH)_2$, BaO_2
Be^{2+}, $Be_2O_2^{-}$	$Be(OH)_2$, BeO, $Be_2O(OH)_2$
Bi^{3+}, $BiOH^{2+}$, BiO^{+}, BiO_2^{-}, BiO_3^{-}	Bi, $Bi(OH)_3$, BiOOH, Bi_2O_3, Bi_2O_5, Bi_4O_7, Bi_2O_4
Ca^{2+}, $CaOH^{+}$	$Ca(OH)_2$, CaO_2, $CaCO_3$, $CaSO_4$
Cd^{2+}, $CdOH^{+}$, $HCdO_2^{-}$	Cd, $Cd(OH)_2$
Ce^{3+}, CeO^{+}, $Ce(OH)^{3+}$, $Ce(OH)_2^{2+}$	$Ce(OH)_3$, CeOOH, $Ce_2(CO_3)_3$, CeO_2
Cm^{3+}, $CmOH^{2+}$, $Cm(OH)_2^{+}$	$Cm(OH)_3$, CmOOH

Contaminant Ion/Ion Adduct	Potentially precipitated by ZVM as
Co^{2+}, $HCoO_2^-$	Co, CoO_2, $Co(OH)_2$, $Co(OH)_3$, CoOOH, CoS
Cr^{n+}, $Cr_2O_7^-$, $Cr_2O_4^{2-}$, CrO_4^{2-}, $HCrO_4^-$, CrO_2^-, CrO_3^{3-}, $CrOH^{2+}$, $Cr(OH)_2^+$, $Cr(OH)_4^-$	Cr, $Cr(OH)_2$, $Cr(OH)_3$, $Cr(OH)_4$, CrOOH, Cr_2O_3
Cs^+	CsO_2
Cu^{n+}, $Cu(OH)^+$, $HCuO_2^-$, CuO_2^{2-}, CuCl2-, $Cu(OH)_2^-$, $Cu(OH)_4^{2-}$	Cu, $Cu(OH)_2$, CuO, Cu_2O, $CuCl_2.3Cu(OH)_2$
Dy^{3+}, $DyOH^{2+}$, DyO^+, DyO_2^-	$Dy(OH)_3$, DyOOH, Dy_2O_3, $Dy_2(CO_3)_3$
Er^{3+}, $ErOH^{2+}$, ErO^+, ErO_2^-	$Er(OH)_3$, ErOOH, Er_2O_3
Eu^{n+}, $EuOH^{2+}$, EuO^+, EuO_2^-	$Eu(OH)_3$, EuOOH, EuO_3H_3, $Eu_2(CO_3)_3$
Fe^{n+}, $FeO_xH_y^{n+/-}$, $FeSO_4^+$, $FeSO_4$, $Fe(SO_4)_2^-$,	Fe_2O_3, Fe_3O_4, $Fe(OH)_x$, FeOOH, $Fe_8O_8(OH)_6SO_4$, $Fe_6(OH)_{12}SO_4$, $FeCO_3$, FeS_2, FeS, $Fe(HS)_2$
Ga^{3+}, $GaOH^{2+}$, GaO^+, GaO_2^-, $HGaO_3^{2-}$, GaO_3^3	$Ga(OH)_3$, GaOOH, Ga_2O_3
Gd^{n+}, $GdOH^{2+}$, GdO^+, GdO_2H, GdO_2^-	$Gd(OH)_3$, GdOOH, Gd_2O_3, $Gd_2(CO_3)_3$
Ge^{2+}, H_2GeO_3, $HGeO_3^-$, GeO_3^{2-}	Ge, $Ge(OH)_2$, GeO, GeO_2
Hf^{4+}, HfO^{2+}, $HHfO_2^-$, $HHfO_3^-$, HfO^{2-}	$Hf(OH)_n$, $HfO(OH)_2$, HfO_2
Hg^{2+}, $HHgO_2^-$, $Hg(OH)_2$	Hg, HgO, HgO_2
Ho^{3+}, $HoOH^{2+}$, HoO^+, HoO_2H, HoO_2^-	$Ho(OH)_3$, HoOOH, Ho_2O_3
In^{3+}, In^+, $InOH^{2+}$, $In(OH)_2^+$, $HInO_2$, InO^+, InO_2^-	In, $In(OH)_3$, InOOH, In_2O_3
Ir^{3+}, IrO_4^{2-}	Ir, IrO_2
La^{3+}, $LaOH^{2+}$, LaO^+, LaO_2H, LaO_2^-	$La(OH)_3$, LaOOH, $La_2(CO_3)_3$, La_2O_3
Lu^{3+}, $LuOH^{2+}$, LuO^+, LuO_2^-	$Lu(OH)_3$, LuOOH, Lu_2O_3
Mg^{n+}, $MgOH^+$	MgO_2, $Mg(OH)_2$, $MgCO_3$
Mn^{2+}, $HMnO_2^-$, MnO_4^-, MnO_4^{2-}, $MnOH^+$, $Mn(OH)_3^-$, $Mn(OH)_4^{2-}$, MnO, MnOH, MnO_2^{2-}	$Mn(OH)_2$, MnO_2, Mn_2O_3, Mn_3O_4, MnS, $MnHCO_3$, $MnCO_3$
Mo^{3+}, $HMoO_4^-$, MoO_4^{2-}, MoO_2^+, H_2MoO_4, MoO_2OH^+	Mo, $Mo(OH)_2$, $Mo(OH)_3$, $Mo(OH)_4$, $MoO(OH)_2$, $MoO(OH)_3$, MoOOH, MoS_2, H_2MoO_4, MoO_2, MoO_3
Nb^{n+}, NbO_2^{n+} $Nb(OH)_5$, NbO_3^-, $HNbO_3$, $Nb(OH)_6^-$	Nb, NbO, NbO_2, Nb_2O_5
Nd^{3+}, $NdOH^{2+}$, NdO^+, NdO_2H, NdO_2^-	$Nd(OH)_3$, Nd_2O_3, NdOOH, Nd_nO_m, $Nd_2(CO_3)_3$
Ni^{2+}, $HNiO_2^-$, NiO_2^{2-}, $Ni(OH)_3^-$, $Ni(OH)_4^{2-}$, $NiOH^+$	Ni, NiO_2, $Ni(OH)_2$, $Ni(OH)_3$, NiS, Ni_3O_4, Ni_2O_3, Ni_2H, Ni_2O_4
Np^{n+}, NpO_2OH, NpO_2OH^+, $NpOH^{3+}$, $Np(OH)_5^-$,$NpO_2OH_2^-$, NpO_2^+, NpO_2^{2+}, NpO_2F^+, NpF_2^{2+}, $NPO_2CO_3^-$, $NpO_2(CO_3)_2^{3-}$, $NpO_2(CO_3)_3^{5-}$	NpO_2, NpO_3, NpO_5, $Np(OH)_4$
OsO_4^{2-}, H_2OsO_5, $HOsO_5^-$, OsO_5^{2-}	Os, OsO_2, OsO_4
Pa^{4+}, $PaOH^{3+}$, $Pa(OH)_2^{2+}$, $Pa(OH)_3^+$, $PaO(OH)_3$, $PaO(OH)_2$, $PaOOH^{2+}$, PaO_2^+	Pa_xO_y, $Pa(OH)_x$
Pb^{2+}, $HPbO_2^-$, PbO_3^{2-}, $PbOH^+$, $HPbO_2^-$, $Pb(OH)_3^-$	Pb, PbO, $Pb(OH)_2$, PbO_2, Pb_2O_3
Pd^{n+}, $PdOH^+$, PdO_2^{2-}, PdO_3^{2-}, $PdCl_4^{2-}$	Pd, Pd_2H, PdO_3, $Pd(OH)_2$, $Pd(OH)_4$
Pm^{3+}	$Pm(OH)_3$, PmOOH, Pm_nO_m
Po^{2+}, $Po(OH)_2^{4+}$, PoO_3^{2-}	Po, PoO_2, PoO_3, H_2PoO_3, $Po(OH)_4$, $PoO(OH)_2$
Pr^{3+}, $Pr(OH)_2^+$, $PrOH^{2+}$, PrO^+, PrO_2H, PrO_2^-	$Pr(OH)_3$, PrOOH, PrO_2, $Pr_2(CO_3)_3$, Pr_2O_3
Pt^{2+}, PtO, $Pt(OH)^{n+}$, PtO_2^{2-}, PtO_4^{2-}	Pt, $Pt(OH)_2$, PtO_2, PtO_3
Pu^{3+}, $PuOH^{2+}$, $PuO_2(OH)_2$, PuO_2^+, PuO^{2+}, PuF_3^+, $PuO_2F_3^-$, $PuO_2(OH)_2H$ CO_3^-,PuO_2OH^+, $Pu(OH)_5^-$	PuO_2, PuO_3, Pu_2O_3, $Pu(OH)_3$, $Pu(OH)_4$
Re^-, Re^+, ReO_4^-	Re, ReO_2, ReO_3, Re_2O_3
Rh^{n+}, $RhOH^+$, RhO, RhO^+, RhO_4^{2-}	Rh, RhO_2, Rh_2O_3
Ru^{3+}, RuO^+, H_2RuO_5, $HRuO_5^-$, $Ru(OH)_2^+$, $Ru(OH)_2^{2+}$, H_2RuO_5, $HRuO_5^-$, RuO_4^{2-}, RuO_4^-, RuO_4^{2-}	Ru, RuO_2, RuO_4, RuOOH, $Ru(OH)_3$
SbO_2^+, SbO^+, SbO_3^-, SbO_2^-, $HSbO_2$	Sb, Sb_2O_5, Sb_2O_3, $HSb(OH)_6$
Sc^{3+}, ScO^+, $HScO_2$, ScO_2^-, $ScOH^{2+}$	$Sc(OH)_3$, ScOOH, Sc_2O_3
H_2Se, HSe^-, SeO_4^{2-}, H_2SeO_3, $HSeO_4^-$, $HSeO_3^-$, SeO_3^{2-}	Se
Sm^{n+}, $SmOH^{2+}$, $Sm(OH)_2^+$, SmO^+, SmO_2^-	Sm_2O_3, $Sm(OH)_3$, SmOOH, $Sm_2(CO_3)_3$
Sn^{2+}, Sn^{4+}, $SnOH^+$, $SnOOH^+$, $Sn(OH)_2^{2+}$, $Sn(OH)_3^+$, $Sn(OH)_5^-$, $Sn(OH)_5^{2-}$, SnO, $HSnO_2^-$, SnO_3^{2-}	Sn, $Sn(OH)_2$, $Sn(OH)_4$, SnO_2
Sr^{2+}, $SrOH^+$	$Sr(OH)_2$, SrO_2
Tb^{3+}, $TbOH^{2+}$, TbO^+, TbO_2H, TbO_2^-	$Tb(OH)_3$, TbOOH, Tb_2O_3, Tb_7O_{12}, Tb_6O_{11}, TbO_2, $Tb_2(CO_3)_3$
Tc^{2+}, TcO_4^-, $TcOOH^+$, $TcOOH_3^-$, $TcO(OH)_2$, $TcO(OH)_3^-$, TcO^{2+}	Tc, Tc_3O_4, TcOH, Tc_4O_7, TcO_2, $Tc(OH)_2$
Te^{2-}, Te^{4+}, H_2TeO_4, $HTeO_4^-$, $Te(OH)_3^+$, TeO_4^{2-}, $HTeO_2^+$, $HTeO_3^-$, TeO_3^-	Te, TeO_2, $TeO_3.3H_2O$, H_2TeO_4
Th^{4+}	$Th(OH)_n$, ThO_2

(*Continued*)

Contaminant Ion/Ion Adduct	Potentially precipitated by ZVM as
Ti^{n+}, $HTiO_3^-$	$Ti(OH)_3$, TiOOH, TiO_2
Tl^{3+}, Tl^+, TlOH, TlO_2^-, $HTlO_2$	Tl, $Tl(OH)_3$, TlOOH, TlOH, Tl_2O_4
Tm^{n+}, $TmOH^{2+}$, TmO^+, TmO_2H, TmO_2^-	$Tm(OH)_3$, TmOOH, Tm_2O_3
U^{n+}, UO_2F^+, UO_2^+, $U(OH)_x^{n+/-}$, $H_2O_{13}U_3^-$, UO_2^{2+}, UO_4^{2-}, HUO_4^-, $H_5O_5U^-$, UO_2^+, $UO_2(OH)_2$, $UO_2(OH)_3^-$, $UO_2(CO_3)_2^{2-}$, $UO_2(CO_3)_3^{4-}$	$U(OH)_4$, UO_2, UO_3, UO_4, U_3O_8, U_4O_9, UF_4, UO_2CO_3
V^{n+}, VO_2^+, VO^{2+}, VOH^{2+}, VO^+, $H_3V_2O_7^-$, $H_2VO_4^-$, HVO_4^{2-}, VO_4^{2-}, $VOOH^+$, $(VO)_2(OH)_5^-$, $V(OH)_m^{n+/-}$, $HV_2O_5^-$	$V(OH)_n$, V_2O_5, V_2O_4, V_2O_3, V_3O_5, V_2O_2
WO_4^{2-}, WO_5^{2-}	W, WO_2, W_2O_5, WO_3
Y^{3+}, YOH^{2+}, YO^+, HYO_2, YO_2^-	$Y(OH)_3$, YO_3H_3, YOOH, $Y_2(CO_3)_3$, Y_2O_3
Yb^{n+}, $YbOH^{2+}$, YbO_2, YbO_2^-	$Yb(OH)_3$, YbOOH
Zn^{2+}, $HZnO_2^-$, $ZnOH^+$, $Zn(OH)_3^-$, $Zn(OH)_4^{2-}$, ZnO_2^{2-}	Zn, ZnS, $Zn(OH)_2$, ZnO_2
Zr^{n+}, ZrO^{2+}, $HZrO_2^+$, $HZrO_3^-$	$Zr(OH)_n$, ZrO_2

APPENDIX 1.C HALF REACTIONS AND REDOX POTENTIALS ASSOCIATED WITH ZVM

All ZVM, when present in the water form redox half cells with the potentials indicated. These form separate hydrogen cells, which interact with the ZVM and ZVM corrosion products (Figs. 1.2 and 1.3). Species that act as cathodes to n-Fe^0 have $E^o < E^o$ Fe^0. Fe^0 can act as both a cathode (Fe^{III}) and an anode (Fe^{II}). Species that act as anodes to n-Fe0 have $E^o > E^o$ Fe. Each ZVM species acts as a cathode or anode to one or more ZVM species present in the water. Figure 1.2 illustrates the dominant corrosion species types associated with the anodic ZVM species. Similar relationships exist between ZVM, hydroxides, oxides, and peroxides (where appropriate) for each species listed in Appendix 1.B and 1.C in the diffusion remediation environment.

Data Source: [131, 176–178]

Half Reaction	E^o(V)	Half reaction	E^o(V)	Half reaction	E^o(V)
$Sr^0 = Sr^+ + e^-$	4.10	$Hf^0 = Hf^{4+} + 4e^-$	1.55	$Ge^0 = Ge^{4+} + 4e^-$	−0.12
$Ca^0 = Ca^+ + e^-$	3.80	$Zr^0 = Zr^{4+} + 4e^-$	1.45	$Ge^0 = Ge^{2+} + 2e^{--}$	−0.24
$Li^0 = Li^+ + e^-$	3.04	$Mn^0 = Mn^{2+} + 2e^-$	1.19	$Re^0 = Re^{3+} + 3e^-$	−0.30
$Cs^0 = Cs^+ + e^-$	3.03	$V^0 = V^{2+} + 2e^-$	1.18	$Bi^0 = Bi^{3+} + 3e^-$	−0.31
$Rb^0 = Rb^+ + e^-$	2.98	$Nb^0 = Nb^{3+} + 3e^-$	1.10	$Cu^0 = Cu^{2+} + 2e^-$	−0.34
$K^0 = K^+ + e^-$	2.93	$Cr^0 = Cr^{2+} + 2e^-$	0.91	$Tc^0 = Tc^{2+} + 2e^-$	−0.40
$Ba^0 = Ba^{2+} + 2e^-$	2.91	$Zn^0 = Zn^{2+} + 2e^-$	0.76	$Ru^0 = Ru^{2+} + 2e^-$	−0.46
$Sr^0 = Sr^{2+} + 2e^-$	2.90	$Cr^0 = Cr^{3+} + 3e^-$	0.74	$Bi^0 = Bi^+ + e^-$	−0.5
$Ca^0 = Ca^{2+} + 2e^-$	2.87	$Ta^0 = Ta^{3+} + 3e^-$	0.60	$Cu^0 = Cu^+ + e^-$	−0.52
$Na^0 = Na^+ + e^-$	2.71	$Ga^0 = Ga^{3+} + 3e^-$	0.55	$Te^0 = Te^{4+} + 4e^-$	−0.57
$Mg^0 = Mg^+ + e^-$	2.70	$Fe^0 = Fe^{2+} + 2e^-$	0.44	$Rh^0 = Rh^{2+} + 2e^-$	−0.60
$La^0 = La^{3+} + 3e^-$	2.38	$Cd^0 = Cd^{2+} + 2e^-$	0.40	$Rh^0 = Rh^+ + e^-$	−0.60
$La^0 = La^{3+} + 3e^-$	2.38	$In^0 = In^{3+} + 3e^-$	0.34	$Tl^0 = Tl^{3+} + 3e^-$	−0.74
$Mg^0 = Mg^{2+} + 2e^-$	2.37	$Tl^0 = Tl^+ + e^-$	0.34	$Rh^0 = Rh^{3+} + 3e^-$	−0.76
$Ce^0 = Ce^{3+} + 3e^-$	2.33	$Co^0 = Co^{2+} + 2e^-$	0.28	$Po^0 = Po^{4+} + 4e^-$	−0.76
$Th^0 = Th^{4+} + 4e^-$	1.90	$Ni^0 = Ni^{2+} + 2e^-$	0.26	$Ag^0 = Ag^+ + e^-$	−0.80
$Be^0 = Be^{2+} + 2e^-$	1.85	$Ga^0 = Ga^+ + e^-$	0.20	$2Hg^0 = Hg_2^{2+} + 2e^-$	−0.80
$U^0 = U^{3+} + 3e^-$	1.80	$Mo^0 = Mo^{3+} + 3e^-$	0.20	$Pd^0 = Pd^{2+} + 2e^-$	−0.95
$Al^0 = Al^{3+} + 3e^-$	1.66	$In^0 = In^+ + e^-$	0.14	$Ir^0 = Ir^{3+} + 3e^-$	−1.16
$Md^0 = Md^{3+} + 3e^-$	1.65	$Fe^0 = Fe^{3+} + 3e^-$	0.04	$Pt^0 = Pt^{2+} + 2e^-$	−1.18
$Ti^0 = Ti^{2+} + 2e^-$	1.63	$H_2 = 2H^+ + 2e^-$	0.00	$Au^0 = Au^{3+} + 3e^-$	−1.50
$Hf^0 = Hf^{4+} + 4e^-$	1.55	$2H^+ + 2e^- = H_2$	0.00	$Au^0 = Au^+ + e^-$	−1.69
$Zr^0 = Zr^{4+} + 4e^-$	1.45	$W^0 = W^{3+} + 3e^-$	−0.10		

REFERENCES

[1] Rosicka D, Sembera J. Assessment of influence of magnetic forces on aggregation of zero-valent iron nanoparticles. Nanoscale Res Lett 2010;6 (10):6.

[2] Kim DH, Kim J, Choi W. Effect of magnetic field on the zero valent iron induced oxidation reaction. J Hazard Mater 2011;192:928–931.

[3] Dalla VE, Coisson M, Appino C, Vinai F, Sethi R. Magnetic characterisation and interaction modelling of zerovalent iron nanoparticles for the remediation of contaminated aquifers. J Nanosci Nanotechnol 2009;9:3210–3218.

[4] Wang Q, Kanei SR, Park H, Ryu A, Choi H. Controllable synthesis, characterisation, and magnetic properties of nano-scale zerovalent iron with high Brunauer-Emmett-Teller surface area. J Nanopart Res 2009;11:749–755.

[5] Huang CP, Wang HW, Chiu PC. Nitrate reduction by metallic iron. Water Res 1998;32:2257–2264.

[6] Liou YH, Lo S-L, Lin C-J, Kuan WH, Weng SC. Effects of iron surface pre-treatment on kinetics of aqueous nitrate reduction. J Hazard Mater 2005;B126:189–195.

[7] Solovyov S, Goldman A. *Mass Transport and Reactive Barriers in Packaging: Theory, Applications & Design*. Lancaster, PA: DES Tech Publications Inc.; 2007. p 558.

[8] Crane RA, Scott TB. Nanoscale zero-valent iron: future prospects for an emerging water treatment technology. J Hazard Mater 2012;211–212:112–125.

[9] Noubactep C. Aqueous contaminant removal by metallic iron: is the paradigm shifting? Water SA 2011;37:419–426.

[10] Antia DDJ. Sustainable zero-valent metal (ZVM) water treatment associated with diffusion, infiltration, abstraction and recirculation. Sustainability 2010;2:2988–3073.

[11] Junyapoon S. Use of zero-valent iron for waste water treatment. KMITL Sci Technol J 2005;5:587–595.

[12] Zhang W-X. Nanoscale iron particles for environmental remediation: an overview. J Nanopart Res 2003;5:323–332.

[13] Ma L, Zhang W-X. Enhanced biological treatment of industrial waste water with bi-metallic zero-valent iron. Environ Sci Technol 2008;42:5384–5389.

[14] Comfort SD, Shea PJ, Machacek TA, Satapanajaru T. Pilot-scale treatment of RDX-contaminated soil with zerovalent iron. J Environ Qual 2003;32:1717–1725.

[15] Loraine G, Burris D, Li L, Schoolfield J. Mass transfer effects on kinetics of dibromoethane reduction by zero valent iron in packed-bed reactors. J Environ Eng 2002;128:85–93.

[16] Zang Y, Jing Y, Quan X, Liu Y, Onu P. A built-in zerovalent iron anaerobic reactor to enhance treatment of azo dye waste water. J Water Sci Technol 2011;63:741–746.

[17] Gavaskar A, Tatar L, Condit W. Cost and performance report: nanoscale zero-valent iron technologies for source remediation. NAVFAC Naval Facilities Engineering Command. Contract Report CR-05-007-ENV. Port Hueneme: Engineering Service Center; 2005. p 44.

[18] Henderson AD, Demond AH. Impact of solids formation and gas production on the permeability of ZVI PRBs. J Environ Sci 2011;137:689–696.

[19] Jeen SW, Amos RT, Blowes DW. Modelling gas formation and mineral precipitation in a granular iron column. Environ Sci Technol 2012;46:6742–6749.

[20] Antia DDJ. Formation and control of self-sealing high permeability groundwater mounds in impermeable sediment: implications for SUDS and sustainable pressure mound management. Sustainability 2009;1:855–923.

[21] Antia DDJ. Polymerisation theory—formation of hydrocarbons in sedimentary strata (hydrates, clays, sandstones, carbonates, evaporates, volcanoclastics) from CH_4 and CO_2: parts I to IV. Indian J Petrol Geol 2009;17(1):49–86; 2009;17(2):11–70; 2010;18(1):1–50; 2011;18(2):1–45.

[22] Antia DDJ. Interpretation of overland flow associated with infiltration devices placed in boulder clay and construction fill. In: Wong TSW, editor. *Overland flow and surface runoff*. New York: Nova Science Publishers; 2012. p 211–285.

[23] Antia DDJ. Interacting infiltration devices (field analysis, experimental observation and numerical modeling): prediction of seepage (overland flow) locations, mechanisms and volumes—implications for SUDS, groundwater raising projects and carbon sequestration projects. In: Hirsch G, Kappel B, editors. *Hydraulic Engineering: Structural Applications, Numerical Modeling and Environmental Impacts*. New York: Nova Science Publishers; 2011. p 85–156.

[24] Westerhof P, James J. Nitrate removal in zero-valent iron packed columns. Water Res 2003;37:1818–1830.

[25] Chen YM, Li CW, Chen SS. Fluidized zero valent iron bed for nitrate removal. Chemosphere 2005;59:753–759.

[26] Hsu J-C, Liao C-H, Wei Y-L. Nitrate removal by synthetic nanoscale zero-valent iron in aqueous recirculated reactor. Sustain Environ Res 2011;21:353–359.

[27] Ji MK, Park WB, Khan MA, Abou-Shanab RA, Kim Y, Cho Y, Choi J, Song H, Jeon BH. Nitrate and ammonium ions removal from groundwater by a hybrid system of zero-valent iron combined with absorbents. J Environ Monit 2012;14:1153–1158.

[28] Anotai J, Liao C-H, Ruangchanikom C. Nitrate removal by Fe^0/CO_2 process using an innovative continuous flow reactor. J Environ Eng Manage 2010;20:77–84.

[29] Cho D-W, Abou-Shnab RAI, Kim Y, Jeon B-H, Song H. Enhanced reduction of nitrate in groundwater by zero-valent iron with activated red mud. Geosyst Eng 2011;14:65–70.

[30] Ginner JL, Alvarez PJJ, Smith SL, Scherer MM. Nitrate and nitrite reduction by Fe^0: influence of mass transport, temperature and denitrifying microbes. Environ Eng Sci 2004;21:219–229.

[31] Liang F, Fan J, Guo Y, Fan M, Wang J, Yang H. Reduction of nitrite by ultrasound-dispersed nanoscale zero-valent iron particles. Ind Eng Chem Res 2008;47:8550–8554.

[32] Zhang Z, Hao Z, Yang Y, Zhang J, Wang Q, Xu X. Reductive denitrification kinetics of nitrate by zero-valent iron. Desalination 2010;257:158–162.

[33] Huang YH, Zhang TC. Nitrite reduction and formation of corrosion coatings in zerovalent iron systems. Chemosphere 2006;64:937–943.

[34] Xu J, Gao N, Tang Y, Deng Y, Sui M. Perchlorate removal using granular activated carbon supported iron compounds: synthesis, characterisation, and reactivity. J Environ Sci 2010;23:1807–1813.

[35] Huang H, Sorial GA. Perchlorate remediation in aquatic systems by zero valent iron. Environ Eng Sci 2007;24:917–926.

[36] Lee C, Batchelor B, Park SH, Han DS, Abdel-Wahab A, Kramer TA. Reduction of perchlorate using zero-valent titanium (ZVT) anode: reaction mechanism. Adv Environ Res 2012;1:37–55.

[37] Lien H-L, Yi CC, Lee Y-C. Perchlorate removal by acidified zero-valent aluminium and aluminium hydroxide. Chemosphere 2010;80:888–893.

[38] Murad E, Taylor RM. The Mossbauer spectra of hydroxycarbonate green rusts. Clay Min 1984;19:77–83.

[39] Ahmed IAM, Shaw S, Benning LG. Formation of hydroxysulphate and hydroxycarbonate green rusts in the presence of zinc using time-resolved in situ small and wide angle X-ray scattering. Min Mag 2008;72:159–162.

[40] Su C, Puls RW. Significance of Iron (II,III) hydroxycarbonate green rust in arsenic remediation using zerovalent iron in laboratory column tests. Environ Sci Technol 2004;38:5224–5231.

[41] O'Loughlin EJ, Burris DR. Reduction of halogenated ethanes by green rust. Environ Toxicol Chem 2004;23:41–48.

[42] Schwertmann U, Fechter H. The formation of green rust and its transformation to lepidocrocite. Clay Min 1994;29:87–92.

[43] Hansen HCB, Taylor RM. Formation of synthetic analogues of double metal-hydroxy carbonate minerals under controlled pH conditions: I. synthesis of pyroaurite and reevesitie. Clay Min 1990;25:161–179.

[44] Hansen HCB, Taylor RM. Formation of synthetic analogues of double metal-hydroxy carbonate minerals under controlled pH conditions: II. synthesis of desautelsite. Clay Min 1991;26:507–525.

[45] Ruby C, Abdelmoula M, Naille S, Renard A, Khare V, Ona-Nguema G, Morin G, Genin J-MR. Oxidation modes and thermodynamics of Fe^{II-III} oxyhydroxycarbonate green rust: dissolution-precipitation versus in situ deprotonation; about fougerite mineral. Geochim Cosmochim Acta 2009;74:953–966.

[46] Hansen HCB, Poulsen IF. Interaction of synthetic sulphate green rust with phosphate and the crystallization of vivianite. Clays Clay Min 1999;47:312–318.

[47] Ahmed IAM, Benning LG, Kakonyi G, Sumoondur AD, Terrill NJ, Shaw S. Formation of green rust sulphate: a combined in situ time-resolved X-ray scattering and electrochemical study. Langmuir 2010;26:6593–6603.

[48] Wilkin R, McNeil MS. Laboratory evaluation of zero-valent iron to treat water impacted by acid mine drainage. Chemosphere 2003;53:715–725.

[49] Wander MCF Environmental redox reactions of iron [PhD thesis]. New York: Stoney Brook University; 2007.

[50] Davesne E, Dideriksen K, Christiansen BC, Sonne M, Ayala-Luis KB, Koch CB, Hansen HCB, Stipp SLS. Free energy of formation for green rust sodium sulphate ($NaFe^{II}_6\ Fe^{III}_3\ (OH)_{18}\ (SO_4)_{2(s)}$). Geochim Cosmochim Acta 2010;74:6451–6467.

[51] Yang C-W. Removal of hydrogen sulphide with nanoscale zero-valent iron from piggery waste water [MSc thesis]. Taiwan: National University Kaoshiung; 2011.

[52] Keenan CR, Sedlak DL. Factors affecting the yield of oxidants from the reaction of nanoparticulate zero-valent iron and oxygen. Environ Sci Technol 2008;42:1262–1267.

[53] Vesselli E, Rizzi M, de Rogatis L, Ding X, Baraldi A, Cornelli G, Savio L, Vattuone L, Rocca M, Fornasiero P, Baldereschi A, Perissi M. Hydrogen assisted transformation of CO_2 on Nickel; the role of formate and carbon monoxide. J Phys Chem Lett 2010;1:402–416.

[54] Gillham RW, O'Hannesian SF. Enhanced degradation of halogenated aliphatics by zero valent iron. Ground Water 1994;32:958–967.

[55] Janda V, Vasek P, Bizova J, Belohlav Z. Kinetic models for volatile chlorinated hydrocarbons removal by zero-valent iron. Chemosphere 2004;54:917–925.

[56] Liu Y, Majetich SA, Tilton RD, Sholl DS, Lowry GV. TCE dechlorination rates, pathways, and efficiency of nanoscale iron particles with different properties. Environ Sci Technol 2005;39:1338–1345.

[57] Ulsamer S. A model to characterize the kinetics of dechlorination of tetrachloroethylene and trichloroethylene by a zero valent iron permeable reactive barrier [MSc thesis]. USA: Worcester Polytechnic Institute; 2011.

[58] Clausen III C, Geiger CL, Sigman M, Fidler R. Safe, in situ methodologies for the destruction of triacetone triperoxide and other explosive peroxides. US Patent 8062442 B1. November 22, 2011.

[59] Nam S, Tratnyek PG. Reduction of azo dyes with zero valent iron. Water Res 2000;34:1837–1845.

[60] Shih Y-H, Tso C-P, Tung L-Y. Rapid degradation of methyl orange with nanoscale zerovalent iron particles. J Environ Eng Manage 2010;20:137–143.

[61] Chen ZX, Jin XY, Chen Z, Megharai M, Naidu R. Removal of methyl orange from aqueous solution using bentonite-supported nanoscale zero-valent iron. J Colloid Interface Sci 2011;15:601–607.

[62] Dombek T, Dolan E, Schultz J, Klarup D. Rapid reductive dechlorination of atrazine by zero valent iron under acidic conditions. Environ Pollut 2001;111:21–27.

[63] Kim G, Jeong W, Choe S. Dechlorination of atrazine using zero valent iron (Fe^0) under neutral pH conditions. J Hazard Mater 2008;155:502–506.

[64] Oh SY, Cha DK, Chiu PC, Kim BJ. Zero-valent iron treatment of RDX-containing and perchlorate containing wastewaters from an ammunition-manufacturing plant elevated temperatures. Water Sci Technol 2006;54:47–53.

[65] Thomas JM, Hernandez R, Kuo CH. Single-step treatment of 2,4-dinitrotoluene via zero-valent metal reduction and chemical oxidation. J Hazard Mater 2008;155:193–198.

[66] Oh SY, Kang SG, Chiu PC. Degradation of 2,4-dinitrotoluene by persulphate activated with zero-valent iron. Sci Total Environ 2010;408:3464–3468.

[67] Schaefer CE, Topoleski C, Fuller ME. Effectiveness of zerovalent iron and nickel catalysts for degrading chlorinated solvents and n-nitrosodimethylamine in natural groundwater. Water Environ Res 2007;79:57–62.

[68] Mitch WA, Sharp JO, Trussell RR, Valentine RL, Alvarez-Cohen L, Sedlak DL. n-nitrosodimethylamine (NDMA) as a drinking water contaminant: a review. Environ Eng Sci 2003;20:389–404.

[69] Clausen C, Geiger C, Sigman M, Fidler R. Degradation of TATP, TNT, and RDX using mechanically alloyed metals. US Patent 8092622 B1. January 10, 2012.

[70] Oh S-Y, Chiu PC, Kim BJ, Cha DK. Enhancing Fenton oxidation of TNT and RDX through pretreatment with zero-valent iron. Water Res 2003;37:4275–4283.

[71] Fuller ME, Schafer CE, Lowey JM. Degradation of explosives-related compounds using nickel catalysts. Chemosphere 2007;67:419–427.

[72] Oh SY, Cha DK, Kim BJ, Chin PC. Transformation of hexahydro 1,3, 5-trinitro-1,3,5-triazine (RDX), octahydroxo-1,3,5,7-tetranitro-1,3,5,7-tetrazocine (HMX), and methylenedinitramine (MDNA) with elemental iron. Environ Toxicol Chem 2005;24:2812–2819.

[73] Echols E. Environmental remediation of TNT using nanoscale zero-valent iron [MSc thesis]. Florida: University of South Florida; 2009.

[74] Cho C, Bae S, Lee W. Enhanced degradation of TNT and RDX by bio-reduced iron bearing soil minerals. Adv Environ Res 2012;1:1–14.

[75] Barreto-Rodrigues M, Silva FT, Paiva TCB. Combined zero-valent iron and Fenton processes for the treatment of Brazilian TNT industry wastewater. J Hazard Mater 2009;165:1224–1228.

[76] Jin Y, Chiu P. Mitigation of irrigation water using zero-valent iron treatment. Patent WO/2011/163346. June 22, 2011.

[77] Chun CL, Hozalski RM, Arnold WA. Degradation of disinfection byproducts by carbonate green rust. Environ Sci Technol 2007;41:1615–1621.

[78] Lin K-S, Chang N-B, Chuang T-D. Fine structure characterisation of zero-valent iron nano-particles for decontamination of nitrites and nitrates in waste water and ground water. Sci Technol Adv Mater 2008;9:025015 9.

[79] Rocca CD, Belgiorno V, Meric S. Overview of in-situ applicable nitrate removal processes. Desalination 2007;204:46–62.

[80] Boussahel R, Harik D, Mammar M, Lamara-Mohamed S. Degradation of obsolete DDT by Fenton oxidation with zero-valent iron. Desalination 2007;206:369–372.

[81] Singh R, Singh A, Misra V, Singh RP. Degradation of lindane contaminated soil using zero-valent iron, nanoparticles. J Biomed Nanotechnol 2011;7:175–176.

[82] Cong X, Xue N, Wang S, Li K, Li F. Reductive dechlorination of organochlorine pesticides in soils from an abandoned manufacturing facility by zero-valent iron. Sci Total Environ 2010;408:3418–3423.

[83] Ghauch A. Rapid removal of flutriafol in water by zero-valent iron powder. Chemosphere 2008;71:816–826.

[84] Thompson JM, Chislom BJ, Bezbaruah AN. Reductive dechlorination of chloroacetanilide herbicide (alachor) using zero-valent iron nanoparticles. Environ Eng Sci 2010;27:227–232.

[85] Suntornchot P, Satapanajaru T, Comfort SD. Application of nano-zerovalent iron for treating metolachor in aqueous solution. World Acad Sci Eng Technol 2010;72:625–628.

[86] Ghauch A. Degradation of benomyl, picloram, and dicamba in a conical apparatus by zero-valent iron powder. Chemosphere 2001;43:1109–1117.

[87] Berendahl JA, Thies TP. Fenton's oxidation of MTBE with zero valent iron. Water Res 2004;38:327–334.

[88] Chang M-C, Shu H-Y, Hsieh W-P, Wang M-C. Using nanoscale zero-valent iron for the remediation of polycyclic aromatic hydrocarbons contaminated soil. J Air Waste Manage Assoc 2005;55:1200–1207.

[89] Chang M-C, Shu H-Y, Hsieh W-P, Wang M-C. Remediation of soil contaminated with pyrene using ground nanoscale zero-valent iron. J Air Waste Manage Assoc 2007;57:221–227.

[90] Kim Y-H, Shin WS, Ko S-O, Kim M-C. Reduction of aromatic hydrocarbons by zero-valent iron and palladium catalyst. In: Zachry T, editor, *Environmental and Waste Management Symposium*; March 28–April 1, 2004; American Chemical Society; 2004. 5 pp. Available at http://ersdprojects.science.doe.gov/ersd/workshop_pdfs/california_2004/p132.pdf. Accessed June 2, 2014.

[91] Sanchez I, Stuber F, Font J, Fortuny A, Fabregat A, Bengoa C. Elimination of phenol and aromatic compounds by zero valent iron and EDTA at low temperature and atmospheric pressure. Chemosphere 2007;68:338–344.

[92] Hori Y, Murata A, Takahashi R. Formation of hydrocarbons in the electrochemical reduction of carbon dioxide at a copper electrode in aqueous solution. J Chem Soc Faraday Trans 1 1985;85:2309–2326.

[93] Hardy LI, Gilham RW. Formation of Hydrocarbons from the reduction of aqueous CO_2 by zero valent iron. Environ Sci Technol 1995;30:57–65.

[94] Deng B, Cambell TJ, Burris DR. Hydrocarbon formation in metallic iron/water systems. Environ Sci Technol 1997;31:1185–1190.

[95] Antia DDJ. Oil polymerisation and fluid expulsion from low temperature, low maturity, over pressured sediments. J Petrol Geol 2008;31:263–282.

[96] Antia DDJ. Hydrocarbon formation in immature sediments. Adv Petrol Expl Dev 2011;1:1–13.

[97] Antia DDJ. Polymerisation theory for a low temperature catalytic formation of petroleum hydrocarbons involving carbon dioxide, methane and hydrogen in sedimentary rocks. J Appl Geochem 2011;13:142–148.

[98] Antia DDJ. Oil reserves attributable to low temperature and high pressure catalytic processes. Indian J Petrol Geol 2011;19 (1):1–44.

[99] Cai K, Phillips DH, Elliott C, Van der Heiden E, Scippo M-L, Muller M, Connolly L. Removal of androgens and estrogens from water by reactive materials. J Water Res Protect 2010;2:990–993.

[100] Smith T, Wychick D. Colloidal iron dispersions prepared via the polymer catalysed decomposition of iron pentacarbonyl. J Phys Chem 1980;84:1621–1629.

[101] Dold B. Basic concepts of environmental geochemistry of sulphide mine-waste. Mineralogia, geoquimica y geomicrobiologia para el manejo ambiental de desechos mineros. XXIV Curso Latino de Metalogina, August22–September 2, 2005, Lima, Peru Colorado: UNESCO-SEG, SEG; 2005. 36 pp.

[102] Dold B. Basic concepts in environmental geochemistry of sulfidic mine-waste management. In: Kumar ES, editor. *Waste Management*. Croatia: Intech; 2010. p 173–198.

[103] Pourbaix M. *Atlas of electrochemical equilibria in aqueous solutions*. Houston: NACE International; 1974.

[104] Verink ED. Simplified procedure for constructing Porbaix diagrams. In: Revie RW, editor. *Uhlig's Corrosion Handbook*. 3rd ed. Hoboken: John Wiley & Sons Inc; 2011.

[105] Thirunavukkarasu OS, Viraraghavan T, Subramanian KS. Arsenic removal from drinking water using granular ferric hydroxide. Water SA 2003;29:161–170.

[106] Giles DE, Mohapatra M, Issa TB, Anad S, Singh P. Iron and aluminium based adsorption strategies for removing arsenic from water. J Environ Manage 2011;92:3011–3022.

[107] Mamindy-Pajany Y, Hurel C, Marmier N, Romeo M. Arsenic (V) adsorption from aqueous solution onto goethite, hematite, magnetite and zero-valent iron: effects of pH, concentration and reversibility. Desalination 2011;281:93–99.

[108] Tanbooncuy V, Grisdanurak N, Liao CH. Background species effect on aqueous arsenic removal by nano-zero-valent iron using fractional factorial design. J Hazard Mater 2012;205–206:40–46.

[109] Duarte AALS, Cardoso SJA, Alcada AJ. Emerging and innovative techniques for arsenic removal applied to a small water supply system. Sustainability 2009;1:1288–1304.

[110] Nikolaidis NP, Dobbs GM, Lackovic JA. Arsenic removal by zero-valent iron: field, laboratory and modelling studies. Water Res 2003;37:1417–1425.

[111] Jain CK, Singh RD. Arsenic removal using adsorptive media treatment process. India Water Week. Water Energy and Food Security: Call for Solutions, April 10–14, 2012 New Delhi: Ministry of Water Resources; 2012.

[112] Gottinger AM, Wild DJ, McMartin D, Moldovan B, Wang D. Development of an iron-amended biofilter for removal of arsenic from rural Canadian prairie potable water. NRCC-53267. Ottawa: National Research Council Canada; 2010. 14 pp.

[113] Noubactep C. Characterizing the reactivity of metallic iron in Fe^0/As-rock/H_2O systems by long-term column experiments. Water SA 2012;38:511–518.

[114] Noubactep C. On the mechanism of microbe inactivation by metallic iron. J Hazard Mater 2011;198:383–386.

[115] Lee C, Kim JY, Lee WII, Nelsom KL, Yoon J, Sedlak DL. Bactericidal effect of zero-valent iron nanoparticles on Escherichia coli. Environ Eng Sci 2008;42:4927–4933.

[116] Keller AA, Garner K, Miller RJ, Leniham HS. Toxicity of nano-zero valent iron to freshwater and marine species. PLoS One 2012;7 (8):e43983.

[117] Mahdy SA, Raheed QJ, Kalaichelvan PT. Antimicrobial activity of zero-valent iron nanoparticles. Int J Mod Eng Res 2012;2:578–581.

[118] Prema P, Selvarani M. Inactivation of bacteria using chemically fabricated zerovalent iron nanoparticles. Int Res J Pharm Sci 2012;3 (1):37–41.

[119] Diao M, Yao M. Use of zero-valent iron nano-particles in inactivating microbes. Water Res 2009;43:5243–5251.

[120] Chunjian S, Jie W, Yan J, Kniel KE, Chiu PC. Removal of viruses and bacteriophages from drinking water using zero-valent iron. Sep Purif Technol 2012;84:72–78.

[121] Jin Y, Chiu P. Filtration media coated with zero-valent metals, their process of making and use. Patent US 2011/0139726 A1. June 16, 2011.

[122] Devi NL, Shihua YICQ. Recent status of arsenic contamination in groundwater of Northeastern India—a review. Rep Opin 2009;1:22–32.

[123] Sevcu A, El-Temsah YS, Joner EJ, Cernik M. Oxidative stress induced microorganisms by zero valent iron nanoparticles. Microbes Environ 2011;26:271–281.

[124] Jin Y, ChiuP. Mitigation of irrigation water using zero valent iron treatment. Patent US2011/0309021 A1. December 22, 2011.

[125] Mahapatra O, Ramaswamy S, Nune SVK, Yadavalli T, Gopalakrishnan C. Corn flake-like morphology of iron nanoparticles and its antibacterial property. J Gen Appl Microbiol 2011;57:59–62.

[126] Rima J, Li QX, Aouuezova L. Generation of free radicals, analytical methods, bacterial disinfections, and oxidative destruction of organic chemicals using zero valent iron and other metals. Patent US 8048317 B2. November 1, 2011.

[127] Jin Y, Chiu P. Removal of microorganisms and disinfection byproduct precursors using elemental iron or aluminium. Patent US8114279. February 14, 2012.

[128] Miranda-Rios M, Luna-Pabello VM, de Velasquez MTO, Barrera-Godinez JA. Removal of Escherichia coli from biological effluents using natural and mineral aggregates. Water SA 2011;37:213–220.

[129] Rodriquez-Maroto JM, Garcia-Herruzo F, Garcia-Rubio A, Gomez-Lahoz C, Vereda-Alonso C. Kinetics of the chemical reduction of nitrate by zero-valent iron. Chemosphere 2009;74:804–809.

[130] Pilling MJ, Seakins PW. *Reaction Kinetics*. Oxford: Oxford University Press; 1995.

[131] Ebbing DD, Gammon SD. *General Chemistry*. Boston: Houghton Mifflin Co.; 2005 (8th ed), 2008 (9th ed), 2012 (10th ed).

[132] Bouniol P. Influence of iron on water radiolysis in cement based materials. J Nucl Mater 2010;403:167–183.

[133] Kasenow M. *Applied Ground-Water Hydrology and Well Hydraulics*. 2nd ed. Colorado: Water Resources Publications, LLC; 2001.

[134] Zheng D, Hunt ER Jr, Running SW. A daily soil temperature model based on air temperature and precipitation for continental applications. Climate Res. 1993;2:183–191.

[135] Antia DDJ. Modification of aquifer pore-water by static diffusion using nano-zero valent metals. Water 2011;3:79–112.

[136] Lee C-L, Jou C-JG. Integrating suspended copper/iron bimetal nanoparticles and microwave irradiation for treating chlorobenzene in aqueous solution. Environ Pollut 2012;1:160–168.

[137] Mueller NC, Braun J, Bruns J, Cernik M, Rissing P, Rickerby D, Nowack B. Application of nanoscale zero valent iron (NZVI) for groundwater remediation in Europe. Environ Sci Pollut Res 2012;19:550–558.

[138] Narayan RS, Suraya Prakash GK, Kindler A. Iron-air rechargeable battery. Patent US 2012/0187918 A1. July 26, 2012.

[139] Tanbonchuy V, Hsu JC, Grisdanurak N, Liao CH. Arsenate removal by nano zero-valent iron in the gas bubbling system. World Acad Sci Eng Technol 2010;41:263–265.

[140] Tanbonchuy V, Hsu JC, Grisdanurak N, Liao CH. Gas-bubbled nano-zero-valent iron process for high concentration arsenate removal. J Hazard Mater 2011;186:2123–2128.

[141] Tanbonchuy V, Liao CH, Grisdanurak N. Arsenic removal by nanoiron in the gas-bubbled aqueous solution. 2011 International Conference on Environment Science and Engineering. Volume 8; IPCBEE; 2011. pp 237–241. Available at www.ipcbee.com/vol8/53-S20011.pdf. Accessed June 2, 2014.

[142] Dong J, Zhao Y, Zhao R, Zhou R. Effects of pH and particle size on kinetics of nitrobenzene reduction by zero-valent iron. J Environ Sci 2010;22:1741–1747.

[143] Taylor RM. Influence of chloride on the formation of iron oxides from Fe(II) chloride. II effect of [Cl] on the formation of Lepidocrocite and its crystallinity. Clays Clay Min 1984;32:175–180.

[144] Olu-Owolabi BI, Ajayi SO. Cation adsorption on goethite-humic acid complex. Sci Iranica 2003;10:329–333.

[145] Hansel CM, Benner SG, Neiss J, Dohnalkova A, Kukkadapu RK, Fendorf S. Secondary mineralization pathways induced by dissimilatory iron reduction of ferrihydrite under advective flow. Geochim Cosmochim Acta 2003;67:2977–2992.

[146] Christiansen BC, Balic-Zunic T, Petit P-O, Frandsen C, Merup S, Geckeis H, Katerinpoulou A, Stipp SLS. Composition and structure of iron bearing, layered double hydroxide (LDH)—green rust sodium sulphate. Geochim Cosmochem Acta 2009;73:3579–3592.

[147] Dong X, Xhang Y, Liu B, Zhen Y, Hu H, Xue G. Double sandwich polyoxometalate and its Fe(II) substituted derivative $[As_2Fe_5Mo_{21}O_{82}]^{17-}$ and $[As_2Fe_6Mo_{20}O_{80}(H_2O)_2]^{16-}$. Inorg Chem 2012;51:2318–2324.

[148] Yan J, Gao J, Long D-L, Miras HN, Cronin L. Self-assembly of a nanosized, saddle-shaped, solution-stable polyoxometallate anion built from pentagonal building blocks: $[H_{34}W_{119}Se_8Fe_2O_{420}]^{54-}$. J Am Chem Soc 2010;132:11410–11411.

[149] Lee C, Keenan CR, Sedlak DL. Polyoxometalate-enhanced oxidation of organic compounds by nanoparticulate zero-valent iron and ferrous iron in the presence of oxygen. Environ Sci Technol 2008;42:4921–4926.

[150] Vila-Nadal L, Mitchell SG, Rodriguez-Fortea A, Miras HN, Cronin L, Poblet JM. Connecting theory with experiment to understand the initial nucleation steps of heteropolyoxometalate clusters. Phys Chem Chem Phys 2011;13:20136–20145.

[151] Zimmerman, AH. *Nickel-Hydrogen Batteries: Principles and Practice*. Aerospace Press, AIAA, El Segundo, 2011.

[152] Lyons MEG, Rebouillat S. Paving the way to the integration of smart nanostructures: part I: nanotethering and nanowiring via material nanotechnology and electrochemical identification. Int J Electrochem Sci 2009;4:481–515.

[153] Rebouillat S, Lyons MEG, Brandon MP, Doyle RL. Paving the way to the integration of smart nanostructures: part II: nanostructured microdispersed hydrated metal oxides for electrochemical energy conversion and applications. Int J Electrochem Sci 2011; 6:5830–5917.

[154] Thaller LH, Zimmerman AH. Overview of the design, development, and application of nickel-hydrogen batteries. NASA/TP-2003-211905. Hanover: NASA Center for Aerospace Information; 2003.

[155] Chen K-F, Li S, Zhang W. Renewable hydrogen generation by bimetallic zero valent iron particles. Chem Eng J 2011;170:562–567.

[156] Reardon EJ. Styles of corrosion and inorganic control on hydrogen pressure buildup. Environ Eng Sci 2005;39:7311–7317.

[157] Zhao C, Reardon EJ. H2 gas charging of zero-valent iron and TCE degradation. J Environ Protect 2012;3:272–279.

[158] Soukup K, Rogut J, Grabowski J, Wiatowski M, Ludwik-Pardala M, Schneider P, Solcova O. Porous iron and ferric oxide pellets for hydrogen storage: texture and transport characteristics. Advances in Control, Chemical Engineering and Mechanical Engineering. WSEAS Press, 2010. pp 99–103. Available at http://www.wseas.us/e-library/conferences/2010/Tenerife/MECHECICON/MECHECICON-19.pdf. Accessed June 2, 2014.

[159] Rogut, J. The potential of nanoscience and nanotechnology in the development of innovative thermochemical processes of separation, purification and compression of hydrogen and carbon dioxide in emerging technologies. *Nanotech Europe* Institute for Energy; 2009. 30 pp. ftp://data.cc-nanochem.de/NanotechEurope2009/167.pdf

[160] Singh A, Al-Raqom F, Klausner J, Petrasch J. Hydrogen production via iron/iron oxide looping cycle. Proceedings of the ASME 2011 5th International Conference on Energy Sustainability; 2011, ES2011-54499, 1–10. Available at http://itme000.louisiana.edu/assign/Solar%20Thermal%20Project/Literature/ASME%20ES%202011/ES2011-54499.pdf. Accessed June 2, 2014.

[161] Gunawardana B, Singhal N, Swedlund P. Degradation of chlorinated phenols by zero valent iron and bimetals of iron: a review. Environ Eng Res 2011;16:187–203.

[162] Mueller NC, Nowack B. Nano zero valent iron—THE solution for water and soil remediation? Report of the Observatory NANO. EMPA; 2010. 34 pp. Available at www.observatorynano.eu

[163] Noubactep C, Care S, Crane R. Nanoscale metallic iron for environmental remediation: prospects and limitations. Water Air Soil Pollut 2012;223:1363–1382.

[164] Chrysochoou M, McGuire M, Dahal G. Transport characteristics of tea green nano-scale zero valent iron as a function of soil mineralogy. Chem Eng Trans 2012;28:6.

[165] Chrysochoou M, Johnston C, Dahal G. A comparative evaluation of hexavalent chromium treatment in contaminated soil by calcium polysulfide and green-tea nanoscale zero valent iron. J Hazard Mater 2012;201–202:33–42.

[166] Bokare AD, Chi W. Zero-valent aluminium for oxidative degradation of aqueous organic pollutants. Environ Sci Technol 2009;43:7130–7135.

[167] Taylor RM, Robbins RG. Treatment of Berkley Pitlake water using the green precipitate process. Proceedings of the 1998 Conference on Hazardous Waste Research*58* Utah, May 18–21, 1998. 1–14. Available at www.engg.ksu.edu/HSRC/98Proceed/

[168] Zang W, Fyfe WS, Barnett RL. A silver-palladium alloy from the Bahia lateritic gold deposit, Carajas, Brazil. Mineral Mag 1992;56:47–51.

[169] Beverskog B, Puigdomenech I. Pourbaix diagrams for the system copper-chlorine at 5–100°C. SKI Rapport 98:19. Swedish Nuclear Power Inspectorate, 1998.

[170] Hu QH, Zavarin M, Rose TP. Effect of reducing groundwater on the retardation of redox-sensitive radionuclides. Geochem Trans 2008;9:12. DOI: 10.1186/1467-4866-9-12.

[171] Davoodi A, Pakshir M, Babaiee M, Ebrahimi GR. A comparative H2S corrosion study of 304L and 316L stainless steels in acidic media. Corrosion Sci 2011;53:399–408.

[172] Hem JD. Chemical equilibria affecting the behaviour of manganese in natural water. Hydrolog Sci J 1963;8:30–37.

[173] Brookins DG. Eh-pH diagrams for the rare earth elements at 25°C and one bar pressure. Geochem J 1983;17:223–229.

[174] Henderson T. Geochemical reduction of hexavalent chromium in Trinity sand aquifer. Ground Water 1994;32:477–486.

[175] Takena, N. Atlas of Eh-pH Diagrams. Geological Survey of Japan Open File Report No 419, 2005. Available at http://www.fssm.ucam.ac.ma/biblioadmin/opac_css/chimie/Atlas_Eh-pH_diagrams.pdf. Accessed June 2, 2014.

[176] Ellis H. *Book of Data*. London: Longman; 1993.

[177] Lide DR. *CRC Handbook of Chemistry and Physics*. 89th ed. Boca Raton: CRC Press; 2008.

[178] Stark JG, Wallace HG. *Chemistry Data Book*. London: Murray; 1982.

[179] Greenlee LF, Torrey JD, Amaro RL, Shaw JM. Kinetics of zero valent iron nanoparticle oxidation in oxygenated water. Environ Sci Technol 2012;46:12913–12920. DOI: 10.1021/es303037k Web publication date 7/11/2012.